
Learning to Solve Quadratic Unconstrained Binary Optimization in a Classification Way

Ming Chen^{1*}, Jie Chun^{1*}, Shang Xiang², Luona Wei³, Yonghao Du¹, Qian Wan⁴,
Yuning Chen^{1†}, Yingwu Chen¹

¹College of Systems Engineering, National University of Defense Technology

²School of Public Administration, Xiangtan University

³College of Electronics and Information Engineering, South-Central Minzu University

⁴National Engineering Research Center of Educational Big Data,
Central China Normal University

{cmself, chunjie0720, xiangshang165, wlnelysion, duyonghao15,
wanq8228}@163.com, cynnudt@hotmail.com, cywnudt@163.com

Abstract

The quadratic unconstrained binary optimization (QUBO) is a well-known NP-hard problem that takes an $n \times n$ matrix Q as input and decides an n -dimensional 0-1 vector x , to optimize a quadratic function. Existing learning-based models that always formulate the solution process as sequential decisions suffer from high computational overload. To overcome this issue, we propose a neural solver called the Value Classification Model (VCM) that formulates the solution process from a classification perspective. It applies a Depth Value Network (DVN) based on graph convolution that exploits the symmetry property in Q to auto-grasp value features. These features are then fed into a Value Classification Network (VCN) which directly generates classification solutions. Trained by a highly efficient model-tailored Greedy-guided Self Trainer (GST) which does not require any priori optimal labels, VCM significantly outperforms competitors in both computational efficiency and solution quality with a remarkable generalization ability. It can achieve near-optimal solutions in milliseconds with an average optimality gap of just 0.362% on benchmarks with up to 2500 variables. Notably, a VCM trained at a specific DVN depth can steadily find better solutions by simply extending the testing depth, which narrows the gap to 0.034% on benchmarks. To our knowledge, this is the first learning-based model to reach such a performance.

1 Introduction

Nonlinear integer programming is a highly challenging subject in mathematical programming and operations research, where the Quadratic Unconstrained Binary Optimization (QUBO) problem is one of the most well-known cases. Due to its extensive applicability and computational intricacies, the QUBO continues to receive widespread attention[1]. The purpose of the QUBO problem is to optimize an unconstrained quadratic function:

$$\max / \min OFV = f(x) = x^\top Qx = \sum_{i=1}^n \sum_{j=1}^n q_{ij} x_i x_j \quad (1)$$

where Q is a symmetric matrix with $n \times n$ coefficients, while x is a binary (0-1) n -dimensional column vector, i.e., $x_i \in \{0, 1\}$, $i = 1, \dots, n$. OFV is short for objective function value.

*These authors contributed equally.

†Correspondence

This simple formulation is able to represent a remarkable spectrum of applications in Combinatorial Optimization (CO), including those from quantum computing [1], asset exchange problem [2], financial analysis [3], transaction settlement [4], set packing problem [5], linear ordering problem [6], etc. A large number of classic graph problems and constrained quadratic problems can be re-casted into QUBO through simple transformations [7, 8, 9, 10], for which QUBO solving methods can be easily applied. From a computational perspective, the QUBO problem belongs to the NP-hard family. Typical solving methods for the QUBO include exact methods and heuristic methods. Due to its NP-hardness, the QUBO is not expected to be solved by any exact method in polynomial time. For this reason, intensive research has been devoted to developing heuristic methods.

In recent years, the research on learning-based Neural CO (NCO) methods for solving CO problems has become a hot topic in this field [11, 12]. This type of data-driven method has strong scalability and high efficiency for problems of different types and scales, as opposed to traditional search-based metaheuristics which often require substantial computational effort when problem size is large. These works typically model the solution of CO problems as a Markov Decision Process (MDP) [13], and then use deep reinforcement learning (DRL) to train an advanced policy network, Pointer Network (PN) [14] and Graph Neural Network (GNN)-based [15] models for instance, to support dynamic decision-making at each MDP step. Despite the remarkable performance of these models in addressing certain classical CO problems such as the Vehicle Routing Problem (VRP) [16], their applications to QUBO encounter significant limitations:

1) PN-based DRL models. PN-based models require problem data represented by a $n \times C$ matrix to satisfy its fixed C embedding channels, where n is the number of tasks and C is a fixed number of features per task. For instance, the Travelling Salesman Problem (TSP) can be represented by n nodes and their coordinates (each node described by an (x, y) pair), forming an $n \times 2$ matrix. Due to such a requirement, PN-based models encounter difficulties in processing $n \times n$ -dimensional input matrix of the QUBO directly since it is not able to handle problem data where both dimensions are variable, resulting in weak scalability of the model for problems of different scales.

2) GNN-based DRL models. Conversely, GNN-based models [15] excel at encoding $n \times n$ graph data by graph embeddings. Despite this advantage, GNNs incur significant computational and storage costs due to the repeated updating of node and edge hidden states at each MDP step, particularly for large problem sizes. For instance, the GNN in [15] requires an $n \times n \times h$ -dimensional hidden matrices to store edge encodings, which is n times the storage of the PN needed at the same hidden size h . Our preliminary tests revealed that the machine we used for this work could not handle the storage demands of GNNs for large-scale instances (see the results of P7000 in Table 1). Additionally, [17] reported that GNNs are not able to compete with greedy heuristics in certain graph combinatorial optimization problems, aligning with our QUBO experimental results.

The limitations encountered by these networks in solving QUBO are closely related to the MDP-solving paradigm attached to them. When addressing QUBO via an MDP, each step involves flipping the assigned value of a selected binary variable (see the top of Figure 1). According to [18], it is critical to evaluate the impact of each flip on the *OFV* to ensure the high quality of the resulting solution. However, the repeated *OFV* evaluation throughout the MDP leads to significant computational overhead, which may be unacceptable for large-scale instances.

Contributions. Given the above limitations, a radical improvement would require revolutionizing the solution paradigm to compensate for the limitations of DRL models by not using MDP and avoiding repeated *OFV* computations. Considering the binary nature of QUBO variables, a novel solution paradigm based on classification is proposed, which can provide the binary values of all variables directly at once, rather than following sequential decision-making to determine values one by one.

To operationalize the concept of this innovative QUBO classification solution paradigm, we propose a Value Classification Model (VCM)³, which is a neural solver comprised of three key components: an Extractor, the Depth Value Network (DVN), for feature extraction; a Classifier, the Value Classification Network (VCN), for solution determination; and a Trainer, the Greedy-guided Self Trainer (GST), for solver training. Based on graph convolutional, DVN exploits the symmetry property of input data of QUBO to efficiently extract the value features, with performance steadily improving as depth increases. These resulting value features of each variable enable VCN to directly generate the solutions in a classification way. For effective model training, we propose the GST, which does not

³The code is available at <https://github.com/cmself100/VCM-QUBO>.

need any prior optimal labels. Extensive experiments demonstrate the effectiveness of the proposed VCM and GST. A well-trained VCM can directly generate near-optimal solutions for QUBO within milliseconds and exhibit remarkable generalization capabilities across both instance sizes and data distributions. For example, a VCM trained on instances of size 10 can produce near-optimal results for instances of size 7,000 in milliseconds. Furthermore, simply by increasing the testing DVN depth, a VCM trained at a specific depth can attain even better solutions. To our knowledge, this represents the first learning-based classification model for solving QUBO with such a performance.

2 Related Works

The literature on QUBO dates back to [19], which introduced pseudo-boolean functions and binary quadratic optimization. Due to the combinatorial complexity, QUBO has been proven NP-hard in 1979 [20]. Over the decades, a large number of methods for solving QUBO have emerged in the literature. The research on exact methods primarily employed branch-and-bound [21, 22, 23, 24, 25] or branch-and-cut [23]. Since the exact methods are prohibitively expensive when applied to large-size instances, various heuristic methods have extensively emerged, which are designed for high-quality solution discovery within acceptable timeframes. Noteworthy ones include Tabu Search (TS) [26, 27, 28], Simulated Annealing (SA) [29], Local Search (LS) [30], Ant Colony Optimization (ACO) [31], Memetic Algorithm (MA) [32] and hybrid algorithms [33].

Recently, learning-based neural CO methods have exhibited significant promise in addressing CO challenges. Successful applications include 3-D Bin Packing Problem [34], Maximum Cut [15, 35], Routing Problems [14, 36, 37, 38, 39, 16, 40, 41], etc. Unlike traditional search-based methods, these approaches aim to autonomously acquire solution policies from a significant amount of problem data. Nevertheless, the integration of these learning-based heuristics into QUBO-specific applications is still in its infancy, with only a handful of studies exploring this direction and they all adopted the solving paradigm based on MDP. Based on PN, [18] designed hand-crafted features, such as row sum, diagonal elements, and *OFV* values. These feature values can only reflect a small number of characteristics of the problem data, making it difficult to characterize the overall picture of the problem, leading to unsatisfactory results. In addition, since this method models the problem solution process as an MDP, it requires repeated calculation of *OFV* values, resulting in low solving efficiency.

3 The Neural Solver VCM

General scheme. The general scheme of our proposed Value Classification Model (VCM) is outlined in Figure 1 at the bottom, with the detailed neural architecture provided in Appendix A. The neural solver VCM comprises three key components: an Extractor, the Depth Value Network (DVN), for feature extraction; a Classifier, the Value Classification Network (VCN), for solution determination; and a Trainer, the Greedy-guided Self Trainer (GST), for solver training.

The Extractor DVN. The Extractor is responsible for automatically grasping variables and their correlation features from Q matrix to support the Classifier. The efficacy of the Extractor essentially determines the performance of the VCM. We notice that the Q matrix is graph-like data. It is known that the Graph Convolutional Network (GCN) [42] is a robust technique for graph representation, which learns hidden layer representations that encode both local graph structure and features of nodes. The extraction of the l -th layer is summarized as $H^{(l+1)} = \sigma(\tilde{D}^{-1/2}(A + I_N)\tilde{D}^{-1/2}H^{(l)}W^{(l)})$. Here, A , I_N , and \tilde{D} are the adjacency matrix, identity matrix, and the degree matrix of the undirected graph \mathcal{G} . $W^{(l)}$ is a layer-specific trainable weight matrix, and $H^{(l)}$ is the matrix of activations in the l -th layer. The core operation in graph convolution is AH . In QUBO, the A is instantiated as Q , while H is the set of extracted features of the variable vector x .

However, directly using GCN as the Extractor for QUBO poses several insurmountable challenges. First, transforming QUBO into a graph typically results in a fully connected Q matrix, leading to n^2 real-valued edges, with each edge q_{ij} directly affecting the *OFV* of the problem. It is essential to manage the extraction of large-scale edges and discern their distinctions. As stated in [43], the graph convolution in GCNs is a special form of Laplacian smoothing, a key factor for their effectiveness. This smoothing could diminish the influence of high-weight edges, which is not required in QUBO since their original weight differences are essential for the model to accurately identify their impact on the objective function. Also, GCN performance significantly degrades when its depth exceeds

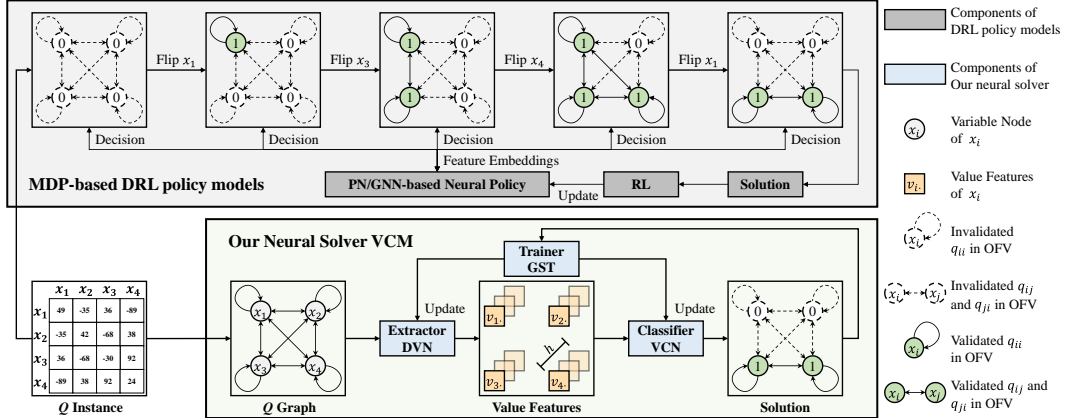


Figure 1: The processes of DRL-based policy models and our QUBO solver. Both PN and GNN-based DRL policy models construct solutions sequentially by capturing environmental embeddings at each step to support decision-making. In contrast, our neural solver VCM outputs solutions directly in a classification way, without any additional decision steps.

two layers [42], even when employing residual connections. This is because when a GCN contains numerous convolutional layers, the resulting output features may become excessively smoothed, making it difficult to differentiate vertices from various clusters. To address these issues and based on the principles of graph convolution, we propose a QUBO-tailored Depth Value Network (DVN).

In QUBO, each variable x_j directly affects the elements of the corresponding j -th row and column in Q . Given that Q is symmetric, i.e., $Q = Q^T$, the features associated with each row should be unified with those of the corresponding column. We first define the features of each variable x_j to be extracted as a value feature, accompanied by a value feature vector $v_j \in \mathbb{R}^h$, where h denotes the hidden size. Let v_j be the value features of the j -th column of Q (denoted as v_j^{col}). Each element in row j can then be expressed as $q_{ij}v_j^{col}$. Consequently, the value features for the i -th row can be computed as $v_i^{row} = \sum_{j=1}^n (q_{ij}v_j^{col})$. To ensure unified row and column features, the value of each column, v_i^{col} , should match the value of its corresponding row, v_i^{row} . This requirement translates to unifying V and QV , where the computation of QV mirrors the core operation of GCN. This alignment may be an additional reason why GCN exhibits effective performance.

In DVN, we take the QV and current V as inputs and employ a learning function \mathcal{F}_E to iterate the value feature. The iteration at depth d is updated as follows:

$$V^{(d+1)} = \mathcal{F}_E(V^{(d)}, QV^{(d)}) \quad (2)$$

Here, $V = \{v_i\}_{i=1}^N$ is the value feature matrix for all variables x (i.e., the nodes in the graph). Each $v_i \in \mathbb{R}^{h \times 1}$ is the value feature vector for x_i with all initial values set to 1. \mathcal{F}_E consists of specific neural networks and activation functions tailored for pattern recognition and features processing. Specifically, it obtains the new value features $V^{(d),D}$ based on the current and QV convolution value features as follows:

$$V^{(d),D} = M_3[V^{(d)}; \tanh(M_2(\text{ReLU}(M_1 Q V^{(d)})))] \quad (3)$$

Where $M_1, M_2 \in \mathbb{R}^{h \times h}$ are learnable memory units that capture specific feature interactions. ReLU and tanh are the activation functions used to filter the extracted features and compress the value features within a limited threshold, respectively. $[;]$ is the horizontal concatenation operator and $M_3 \in \mathbb{R}^{h \times 2h}$ is a learnable memory unit that connects the current and convolution value features. Finally, $V^{(d+1)}$ is then obtained as follows.

$$V^{(d+1)} = \tanh(V^{(d),D}) \quad (4)$$

The output value of tanh, within a symmetric range of $[-1, 1]$, can effectively represent the features of distinct variables. An ablation study on activation functions and memory units demonstrates the

effectiveness of our neural architecture design (see Appendix E). These filtering and compression processes allow DVN to iteratively extract features from Q at any depth, which effectively avoids the problem of decreased performance caused by the convolutional layer increase of GCN. Additionally, during data initialization, we scale the data by λQ to enhance the efficiency of value compression (see Appendix A), where λ represents the scaling factor with a specific value. Experimental results verify that the performance of our solver steadily improves when the iteration depth of the DVN increases. Notably, without incurring additional training costs, our solver can find better solutions simply by extending the iteration depth (see Section 4.3).

The Classifier VCN. Based on the obtained value features $\mathbf{V}^{(d),D}$, we propose a Value Classification Network (VCN) which serves as the classifier to generate the solution x for the QUBO.

$$x = \mathcal{F}_C(\mathbf{V}^{(d),D}) \quad (5)$$

Where \mathcal{F}_C is a learning function that maps the value feature of each variable into a binary value. To this end, we calculate the state of each x_i and use the activation function \tanh to obtain the state of each x_i . The classification result is then determined based on the state of x_i .

$$\{state_i\}_{i=1}^n = \tanh(\mathbf{u} \tanh(\mathbf{M}_4 \mathbf{V}^{(d),D})) \quad (6)$$

$$x_i = \begin{cases} 1, & state_i > 0 \\ 0, & state_i \leq 0 \end{cases} \quad (7)$$

Where $\mathbf{M}_4 \in \mathbb{R}^{h \times h}$ is a learnable memory unit and $\mathbf{u} \in \mathbb{R}^{1 \times h}$ is the learnable uniform vector to integrate the value features of each variable. VCN can produce a complete solution directly by simultaneously considering all variables through a single classification action. Compared to other DRL policy models that rely on sequential decisions, our solver can significantly reduce the computational complexity from $O(kn^2)$ (where the sequence length k can potentially expand to 2^n when the flip of all variables is enumerated) to $O(n^2)$.

The Trainer GST. It is known that the classification model usually requires labeled solutions for training. Unfortunately, in the case of QUBO, acquiring optimal solutions is rather expensive and may be infeasible for large-size problems. For this reason, we propose a Greedy-guided Self Trainer (GST), which effectively avoids the need for pre-labeled optimal solutions. The GST is outlined in Algorithm 1 and its working logic is shown in Figure 2, which consists of three components: a VCM, a Batch Greedy Flip (BGF) algorithm, and a historical best solution set (HB) X^L , where the BGF and HB are two featured ingredients of the GST.

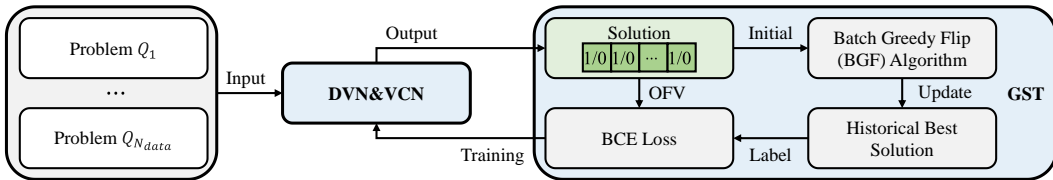


Figure 2: Working logic of the GST.

The Greedy Flip algorithm employs a flip operation to change the assignment for each variable x_i between 0 and 1 (detailed in Appendix B.1). At each step, the algorithm first calculates the Objective Function Value Increment (OFI) for each variable, which quantifies the change of OFV resulting from flipping x_i (detailed in Appendix B.2). The flip operation with the highest positive OFI is selected. The above process continues until all variables are processed. However, computing the OFI at each step is computationally expensive, making it impractical for batch training.

To overcome this computational bottleneck, we propose a batch OFI calculation technique (detailed in Appendix B) that leverages matrix computation acceleration to significantly enhance efficiency. Based on this, we develop a Batch Greedy Flip (BGF) method (detailed in Appendix C), a GPU-accelerated heuristic that improves on the VCM (termed VCM-BGF) by identifying and correcting obvious sub-optimal classification in the current VCM solution.

Algorithm 1 The Greedy-guided Self Trainer

Input: The training dataset D with N_{data} instances, the epoch size E , the batch size B , the training steps per epoch $N_{steps} = \text{ceil}(N_{data}/B)$
Output: The trained VCM with parameters θ^*
Initialize the VCM parameters θ , Adam optimizer and the label set $X_{steps}^L = X_1^L \cup \dots \cup X_{N_{steps}}^L$
for $epoch = 1$ **to** E **do**
 for $step = 1$ **to** N_{steps} **do**
 $data_{step} \leftarrow \text{SampleInput}(D)$
 $X_{step}^L \leftarrow \text{SampleInput}(X_{steps}^L)$
 $state_{step}, X_{step}^{VCM} \leftarrow \text{VCM}(data_{step})$
 $X_{step}^G \leftarrow \text{BatchGreedyFlip}(X_{step}^{VCM}, data_{step})$
 $X_{step}^L \leftarrow \arg \max_{X \in \{X_{step}^G, X_{step}^L\}} OFV(X)$
 $Loss \leftarrow \text{BCELoss}(X_{step}^L, (state_{step} + 1)/2)$
 $\theta \leftarrow \text{Adam}(\theta, Loss)$
 end for
end for

Finally, we introduce a historical best solution set X^L . During the multi-epoch training process, the training dataset is fixed, ensuring that each instance is used once in each training epoch. This allows us to use the VCM-BGF solution X^G at each epoch to maintain and update the historical best solution set X^L . The updated historical best solutions serve as the training labels for our neural solver. This VCM-based, data-driven label-generating process yields adaptive, high-quality labels at low cost. The Binary Cross Entropy (BCE) is applied to calculate the training loss, with the optimization handled by the well-known Adam optimizer [44].

4 Experiments

4.1 Experimental Details

Datasets. The datasets used in our experiments include generated instances (G), benchmarks (B), and well-known instances (P), described in the format: dataset+instance size+(number of instances). For the G set, the Q matrix is uniformly generated at random within [-100,100], following the benchmark data format. The B set is B2500(10) consisting of ten ORLIB instances of size 2500 [45]. The P set includes 21 very-large instances [46] including P3000(5), P4000(5), P5000(5), P6000(3), and P7000(3). The average OFV gap to the current optimal baseline (GAP in %) and the average running time (ART in milliseconds for default, ms) are used as the evaluation indicators.

Parameter setting. Following the Parameters Study (see Appendix F), the default values for VCM parameters are set as $h = 128$, $\alpha = 4$, and $d = 40$. VCM is trained for 100 epochs under four sets of small-size instances (with 10, 20, 50, and 100 variables) with a batch size of 512, resulting in 400 VCMs. Each set includes 512,000 G instances (limited by memory). For fair validation, the test batch size is fixed at 1. Each model is initialized with Xavier initialization [47], and the Adam optimizer is applied with a 10^{-4} learning rate and 0.975 decay factor. Experiments were run on an NVIDIA GeForce RTX 3090 and an Intel i9-9900K CPU with 64GB RAM and Ubuntu 18.04 using Pytorch 1.90 in a Python 3.7 environment.

Competitors. Our evaluation includes several types of competitors: 1) The exact optimizer Gurobi [48]. We set the max allowed time to 1s and 1h. 2) Heuristic classification methods, Diag and SR, proposed in [18]. 3) Heuristic construction algorithm BGF, part of GST. 4) The physics-inspired neural solver, PI-GNN [49], with varying numbers of layers. 5) Three learning-based sequential-decision construction models: one PN-based model called DRLH [18] (which is the state-of-the-art), two GNN-based models called S2V-DQN [15] and ECO-DQN [35] (which are the most relevant state-of-the-art models for solving optimization problems over graphs). These models use the same parameter setting as VCM and are accelerated by our batch OFI calculation technique, resulting in competitors DRLH-B, S2V-DQN-B, and ECO-DQN-B. To assess the stability of VCM, we also include its enhanced version VCM-BGF as a competitor. In addition, for each instance of the datasets, we obtain a high-quality reference solution using an integrated model (called VCM-BGF-HB)

composed of 400 trained VCM-BGFs under depth $d = 100$. VCM-BGF-HB is deemed a high-quality baseline since it is able to achieve an average 0.012% deviation from benchmark optimality (see Table 1).

4.2 Experimental Results

We use the B set and P set to validate the performance of the trained VCMs. The results in Table 1 show that PN-based DRLH-B requires seconds to obtain suboptimal solutions. In terms of solution quality, DRLH-B is outperformed by the ECO-DQN-B, yet it incurs substantial time increases and computational costs due to graph embedding, resulting in an insurmountable GPU memory limitation to preclude their execution on P7000. Among the learning-based competitors, the 2-layer PI-GNN demonstrates the best performance in terms of solution quality. Interestingly, our proposed BGF easily outperforms these learning-based models in both solution quality and speed. Yet it is still dominated by the VCM which is the best solver. Indeed, it surpasses all competitors across the whole instance set in both quality and computational efficiency with the highest Wilcoxon P-value of 3.09E-03 (see Appendix D). Taking VCM50 as an example, it can achieve near-optimal solutions with an average gap of only 0.362% within 8ms for benchmarks. Such a solution speed is rather impressive. The results of the very large instances from the P set show that our proposed VCM maintains near-optimal performance. Particularly, the VCM trained on instances with 10 variables achieves an average gap of 0.569% on P7000, displaying significant generalization ability. The results of the VCM-BGF-HB and Gurobi are also presented as a reference to the VCM. They produce optimal or near-optimal solutions. However, Gurobi can only solve problems in a sequential way and incurs substantial time cost (over 1h for each G100 instance in Appendix G).

Table 1: Results on benchmarks and large well-known instances.

ALGORITHM	OBJECTIVE FUNCTION VALUE BASELINE (OPTIMAL)											
	B2500(10)		P3000(5)		P4000(5)		P5000(5)		P6000(3)		P7000(3)	
	GAP (%)	ART (ms)	GAP (%)	ART (ms)	GAP (%)	ART (ms)	GAP (%)	ART (ms)	GAP (%)	ART (ms)	GAP (%)	ART (ms)
DIAG	81.842	0.7	99.262	1.7	97.374	2.9	98.256	4.4	99.273	11.1	98.843	14.3
SR	26.867	0.1	32.861	0.0	33.510	0.1	33.428	0.2	33.679	0.0	32.758	0.4
VCM10	0.368	7.8	0.566	7.9	0.440	8.1	0.508	8.5	0.645	8.8	0.569	9.1
VCM20	0.488	7.7	0.598	7.9	0.673	8.1	0.657	8.3	0.712	8.6	0.646	9.1
VCM50	0.362	7.7	0.861	7.9	0.669	8.1	0.783	8.1	0.806	8.7	0.702	9.1
VCM100	0.401	7.8	0.763	7.9	0.668	8.0	0.803	8.0	0.914	8.7	0.772	9.1
BGF	0.807	800.8	0.979	984.4	0.834	999.4	0.914	994.7	0.966	999.9	0.730	983.6
DRLH-B	1.640	1.5E+03	2.044	2.4E+03	1.884	5.0E+03	1.853	8.9E+03	2.030	1.5E+04	1.825	2.2E+04
S2V-DQN-B	21.657	1.6E+04	13.172	2.7E+04	13.255	6.3E+04	14.050	1.2E+05	14.403	2.1E+05	-	-
ECO-DQN-B	0.937	2.8E+04	1.371	5.4E+04	1.333	1.2E+05	1.270	2.3E+05	1.467	4.0E+05	-	-
VCM10-BGF	0.230	40.8	0.382	70.6	0.297	107.4	0.322	196.3	0.374	444.4	0.335	613.6
VCM20-BGF	0.227	52.3	0.260	87.8	0.342	135.8	0.310	282.6	0.316	506.8	0.312	634.7
VCM50-BGF	0.136	44.1	0.277	100.2	0.214	170.0	0.262	326.0	0.267	523.3	0.224	770.2
VCM100-BGF	0.139	49.2	0.203	106.0	0.178	186.7	0.245	298.2	0.271	549.7	0.212	770.4
PI-GNN(2-LAYER)	1.689	4.4E+04	2.13	6.2E+04	1.636	7.1E+04	1.418	8.6E+04	1.986	1.1E+05	1.437	1.6E+05
PI-GNN(3-LAYER)	1.909	5.7E+04	2.523	7.2E+04	2.092	8.0E+04	1.945	1.0E+05	2.18	1.3E+05	2.076	1.9E+05
PI-GNN(5-LAYER)	3.28	1.2E+05	3.047	1.0E+05	2.761	1.1E+05	2.463	1.3E+05	2.584	1.8E+05	2.289	2.7E+05
GUROBI-1S	0.034	1.0E+03	0.070	1.0E+03	0.108	1.0E+03	0.091	1.0E+03	0.122	1.0E+03	0.145	1.0E+03
GUROBI-1H	0.0023	3.6E+06	0.0028	3.6E+06	0.0109	3.6E+06	0.0096	3.6E+06	0.0144	3.6E+06	0.0169	3.6E+06
VCM-BGF-HB	0.012	1.9E+04	0.020	3.6E+04	0.027	6.0E+04	0.040	1.1E+05	0.030	2.0E+05	0.057	2.8E+05

¹ The **Bold** indicates the best average result in different classes of methods.

To further investigate the generalization ability of the VCM, we conduct experiments on an additional 1,000 generated G instances with 20, 50, 100, 200, 500, and 1,000 variables. We use VCM-BGF-HB as the optimal baseline. The results, illustrated in Figure 3 and detailed in Appendix G, demonstrate that a VCM trained at a specific size performs well on instances of other sizes. For example, the gap between VCM10 and VCM100 on G100 instances is merely 0.056%, demonstrating the remarkable generalization ability of VCM. The results also show that BGF can further enhance the performance of the VCM, with a solution quality improvement of 0.27% on average. Meanwhile, this improvement afforded by BGF is limited, reflecting the inherent stability of VCM.

In comparison to MDP-based methods, VCM replaces this complex sequential decision-making process with a simple classification process, providing an inherent advantage in solving efficiency that becomes more pronounced as the instance size increases. Notably, the VCM achieves this performance without using OFI (which is essential in sequential decision-based methods), thereby

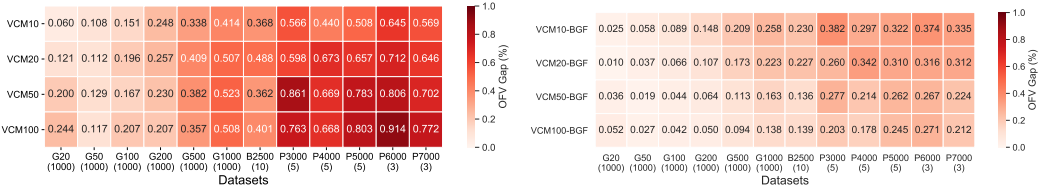


Figure 3: The size generalization ability of VCM and VCM-BGF under different datasets.

considerably reducing computational overhead. The computing time is thousands of times less on average. Also, the computing time increases moderately as the problem size enlarges (see Figure 4). Across the whole datasets (with variables ranging from 20 to 7000), the computing time is always under 10ms. In contrast, other sequential-decision competitors, especially GNN-based models, exhibit excessive time growth as the problem size grows, since the number of decision-making steps increases significantly.

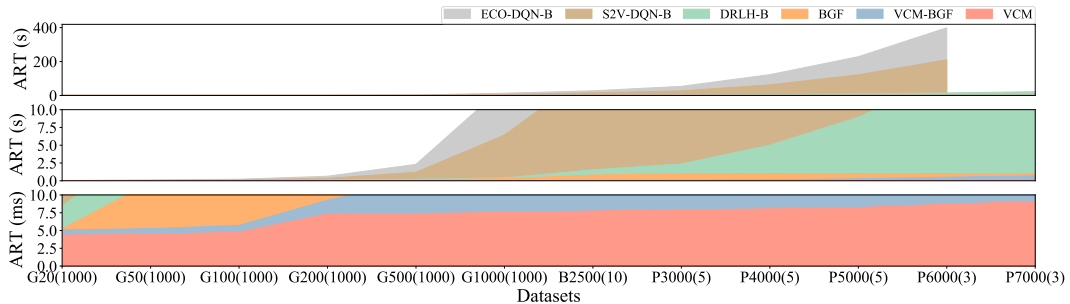


Figure 4: Average running time of different datasets in seconds and milliseconds.

4.3 Model Study

Efficiency of GST. We introduce three training competitors, UnS [49], LHB, and LGF, to validate our Trainer GST. The UnS is an unsupervised training method that directly uses the optimization objective function as the loss function and relaxes the 0-1 variables for optimization. The labels for LHB are obtained by VCM-BGF-HB. The LHB can be considered supervised learning with optimal labels. The labels for LGF are obtained using the current VCM-BGF, which is GST without the historical best solution set. We adopt VCM-BGF-HB as the optimal baseline and illustrate the training curves in Figure 5. The results indicate that GST outperforms competitors in terms of both efficiency and stability. Specifically, GST demonstrates a more efficient and stable training process compared to the unsupervised trainer UnS, which suffers from considerable fluctuations. GST achieves the same performance as the supervised LHB in the early stages of the training process while requiring at least 50% fewer epochs. Although LGF can reach local optimum from time to time, its training process experiences fluctuations due to the unstable quality of the labels outputted by VCM-BGF alone. Therefore, the integration of BGF and historical solutions within GST enables a rapid, stable, and adaptive formation of VCM, and circumvents the substantial costs associated with supervised learning.

Distribution Generalization of VCM. The G set, whose default distribution is denoted as R-1, with all elements of the matrix non-zero. To assess the generalization ability of VCM across diverse data distributions, we generate new datasets by following a standard normal random distribution (RN-1) and deactivating the matrix elements to 0 with probabilities of 10% (R-0.9), 40% (R-0.6), 70% (R-0.3), and 90% (R-0.1). We conduct tests on these instances of diverse distributions with 20, 50, and 100 variables using our trained corresponding-sized VCMs. For each distribution, we generate 1,000 G instances and apply VCM-BGF-HB as the optimal baseline to measure the gap. The results (summarized in Figure 6 and detailed in Appendix H) demonstrate that VCM maintains

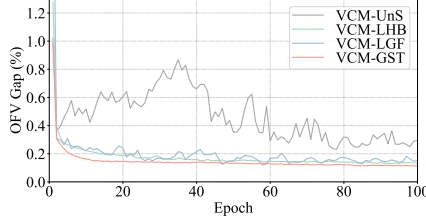


Figure 5: VCM training process under different methods at instance size 50.

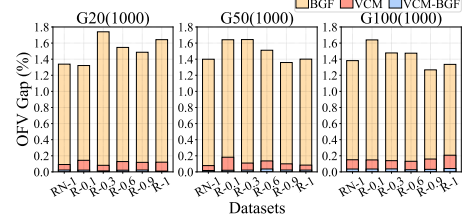


Figure 6: VCM results under different distribution instances.

near-optimal across various data distributions. The VCM performance on the R-0.1 instance set with 100 variables, where 90% Q matrix elements are zero, manages to sustain a performance gap no larger than 0.15%. Besides, since the MaxCut problem can be re-casted into UQBO, with the difference in the data distribution, we extend our evaluation to MaxCut benchmarks to validate our findings. Results detailed in Appendix I further confirm the practical applicability of VCM. These observations imply that the Extractor in VCM can be considered a generic module with distribution-independent and problem-specific in QUBO, thereby bringing VCM a remarkable generalization ability and wide-spread applicability.

The Study of DVN Depth. The depth is crucial for ensuring interaction and coherence between row and column features in DVN graph convolution. As shown in the Parameter Study in Appendix F.2, increasing the training depth of DVN improves feature extraction precision, leading to consistent enhancement in VCM performance. It is logical to hypothesize that a VCM trained at a particular depth d would perform better at deeper testing depths. To investigate this hypothesis, we evaluate six VCMs on benchmark B2500 across eight testing depths. The results (illustrated in Figure 7(a) and detailed in Appendix J) show that all VCMs exhibit significant performance gains as testing depth increases. Even at the training depth of 10, VCM already learns an iterative feature extraction pattern. However, when the testing depth retracts below the training depth, VCM presents a perceptible but tolerable performance degradation, reinforcing the premise that reaching the training depth threshold is essential for DVN stabilization.

To further investigate the rationale behind this performance, we apply the t-SNE [50] on the output $V^{(d),D}$ of Extractor DVN from the trained VCM50- d 10 with varying testing depths. Figure 8 shows that as d increases, clustering transitions into binary clusters gradually. When $d = 1$, it converges to a number of lines, and when $d > 100$, the binary clustering occurs. This demonstrates that our DVN overcomes the limitation of GCN (i.e., its performance degrades as the depth increases, as shown in our evaluation in Appendix K), thus effectively supporting the Classifier VCN. For instance, the default VCM50- d 40 achieves an average gap of merely 0.034% when the testing d hits 300, as opposed to its original gap of 0.362%. This performance enhancement can be generalizable to very large instances, as demonstrated by our evaluations on well-known instances (see Appendix J) and G instance with 10,000 and 20,000 variables (see Appendix L), and is achieved without additional training costs. As shown in Figure 7(b), the computational time increases linearly (on average 0.17ms per depth) as the testing depth enlarges, which verifies the remarkable performance of the VCM and extends its applications.

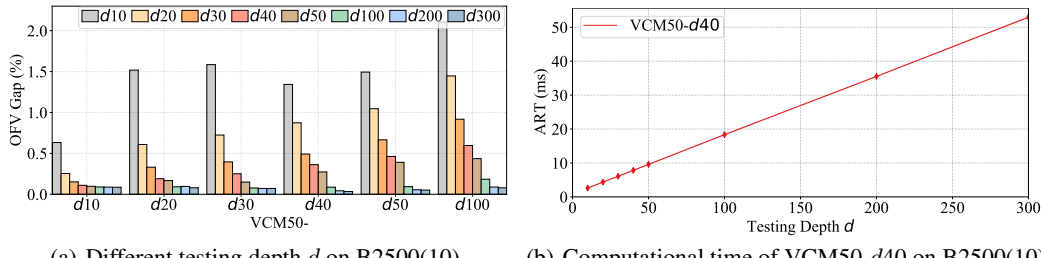


Figure 7: VCM results under different testing depth d .

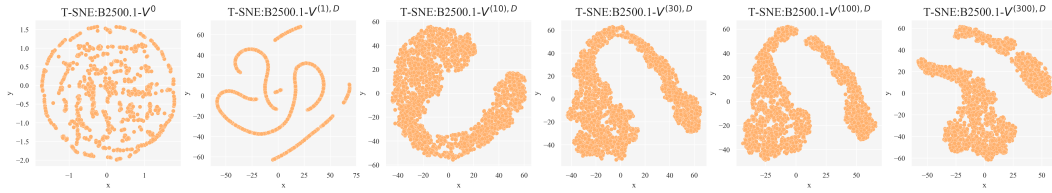


Figure 8: The t-SNE visualizations of $V^{(d),D}$ on the first instance of B2500 under VCM50-d10.

5 Conclusions and Future Work

Our neural solver VCM is a new state-of-the-art learning-based model designed for efficiently solving QUBO from a classification perspective. It applies the Extractor DVN based on graph convolution and exploits the symmetry property in Q to auto-grasp value features. Utilizing these resultant value features of each variable, VCM generates solutions directly through the Classifier VCN in a classification way. Trained by a highly efficient model-tailored Trainer GST which does not require any priori optimal labels, VCM shows near-optimality, high efficiency, and generalization ability in problem-solving. In particular, it can achieve an average gap to benchmark optimality of 0.362% in milliseconds and steadily narrow it down to 0.034% by simply extending the testing depth, which brings only a linearly increased computational time (average 0.17ms per depth).

Although VCM reaches such a performance by single classification decision-making, its optimality may be potentially limited by the VCN utilization of value features from DVN. This limitation poses challenges in achieving the optimal solution. Future research could explore enhancing VCM capabilities, including the development of more accurate classification networks and more efficient trainers, as well as adapting it to address other combinatorial optimization problems and real-world applications.

Acknowledgments and Disclosure of Funding

This work was supported in part by the National Natural Science Foundation of China (No. 72271240, 72201272, 62307015 and 62437002); in part by the Natural Science Foundation of Hunan Province (No. 2022JJ30671 and 2024JJ4047); in part by the Hubei Provincial Natural Science Foundation of China (No. 2024AFB169, 2023AFB295 and 2023AFA020); in part by the China Postdoctoral Science Foundation (No. 2023M741304); and in part by the Scientific Research Foundation of Hunan Provincial Education Department (No. 22C0050).

References

- [1] Fred Glover, Gary Kochenberger, Rick Hennig, and Yu Du. Quantum bridge analytics i: a tutorial on formulating and using qubo models. *Annals of Operations Research*, 314(1):141–183, 2022.
- [2] Fred Glover, Gary Kochenberger, Moses Ma, and Yu Du. Quantum bridge analytics ii: Qubo-plus, network optimization and combinatorial chaining for asset exchange. *Annals of Operations Research*, 314(1):185–212, 2022.
- [3] Seo Woo Hong, Pierre Miasnikof, Roy Kwon, and Yuri Lawryshyn. Market graph clustering via qubo and digital annealing. *Journal of Risk and Financial Management*, 14(1):34, 2021.
- [4] Lee Braine;Daniel J. Egger;Jennifer Glick;Stefan Woerner. Quantum algorithms for mixed binary optimization applied to transaction settlement. *IEEE Transactions on Quantum Engineering*, pages 1–8, 2021.
- [5] Bahram Alidaee, Gary Kochenberger, Karen Lewis, Mark Lewis, and Haibo Wang. A new approach for modeling and solving set packing problems. *European Journal of Operational Research*, 186(2):504–512, 2008.
- [6] Mark Lewis, Bahram Alidaee, Fred Glover, and Gary Kochenberger. A note on xqx as a modelling and solution framework for the linear ordering problem. *International Journal of Operational Research*, 5(2):152–162, 2009.

[7] Iain Dunning, Swati Gupta, and John Silberholz. What works best when? a systematic evaluation of heuristics for max-cut and qubo. *INFORMS Journal on Computing*, 30(3):608–624, 2018.

[8] Gary Kochenberger, Jin-Kao Hao, Fred Glover, Mark Lewis, Zhipeng Lü, Haibo Wang, and Yang Wang. The unconstrained binary quadratic programming problem: a survey. *Journal of combinatorial optimization*, 28:58–81, 2014.

[9] Endre Boros and Peter L Hammer. Pseudo-boolean optimization. *Discrete applied mathematics*, 123(1-3):155–225, 2002.

[10] Pierre Hansen. Methods of nonlinear 0-1 programming. In *Annals of Discrete Mathematics*, volume 5, pages 53–70. Elsevier, 1979.

[11] Cong Zhang, Yaxin Wu, Yining Ma, Wen Song, Zhang Le, Zhiguang Cao, and Jie Zhang. A review on learning to solve combinatorial optimisation problems in manufacturing. *IET Collaborative Intelligent Manufacturing*, 5(1):e12072, 2023.

[12] Zhixiao Xiong, Fangyu Zong, Huigen Ye, and Hua Xu. Neuralqp: A general hypergraph-based optimization framework for large-scale qcqp, 2024.

[13] Richard S Sutton and Andrew G Barto. Reinforcement learning: An introduction. *Robotica*, 17(2):229–235, 1999.

[14] Oriol Vinyals, Meire Fortunato, and Navdeep Jaitly. Pointer networks. *Advances in neural information processing systems*, 28, 2015.

[15] Elias Khalil, Hanjun Dai, Yuyu Zhang, Bistra Dilkina, and Le Song. Learning combinatorial optimization algorithms over graphs. *Advances in neural information processing systems*, 30, 2017.

[16] Jianan Zhou, Yaxin Wu, Wen Song, Zhiguang Cao, and Jie Zhang. Towards omni-generalizable neural methods for vehicle routing problems. *arXiv preprint arXiv:2305.19587*, 2023.

[17] Maria Chiara Angelini and Federico Ricci-Tersenghi. Modern graph neural networks do worse than classical greedy algorithms in solving combinatorial optimization problems like maximum independent set. *Nature Machine Intelligence*, 5(1):29–31, 2023.

[18] Ming Chen, Yuning Chen, Yonghao Du, Luona Wei, and Yingwu Chen. Heuristic algorithms based on deep reinforcement learning for quadratic unconstrained binary optimization. *Knowledge-Based Systems*, 207:106366, 2020.

[19] Peter L Hammer and Sergiu Rudeanu. Pseudo-boolean programming. *Operations Research*, 17(2):233–261, 1969.

[20] Panos M Pardalos and Somesh Jha. Complexity of uniqueness and local search in quadratic 0–1 programming. *Operations research letters*, 11(2):119–123, 1992.

[21] VP Gulati, SK Gupta, and AK Mittal. Unconstrained quadratic bivalent programming problem. *European Journal of Operational Research*, 15(1):121–125, 1984.

[22] Francisco Barahona, Michael Jünger, and Gerhard Reinelt. Experiments in quadratic 0–1 programming. *Mathematical Programming*, 44(1-3):127–137, 1989.

[23] Christoph Helmberg and Franz Rendl. Solving quadratic (0, 1)-problems by semidefinite programs and cutting planes. *Mathematical programming*, 82:291–315, 1998.

[24] Panos M Pardalos, Oleg A Prokopyev, and Stanislav Busygin. Continuous approaches for solving discrete optimization problems. *Handbook on modelling for discrete optimization*, pages 39–60, 2006.

[25] Hong-Xuan Huang, Panos M Pardalos, and Oleg A Prokopyev. Lower bound improvement and forcing rule for quadratic binary programming. *Computational Optimization and Applications*, 33:187–208, 2006.

[26] Yang Wang, Zhipeng Lü, Fred Glover, and Jin-Kao Hao. Effective variable fixing and scoring strategies for binary quadratic programming. In *Evolutionary Computation in Combinatorial Optimization: 11th European Conference, EvoCOP 2011, Torino, Italy, April 27-29, 2011. Proceedings 11*, pages 72–83. Springer, 2011.

[27] Yang Wang, Zhipeng Lü, Fred Glover, and Jin-Kao Hao. Backbone guided tabu search for solving the ubqp problem. *Journal of Heuristics*, 19:679–695, 2013.

[28] Jialong Shi, Qingfu Zhang, Bilel Derbel, and Arnaud Liefooghe. A parallel tabu search for the unconstrained binary quadratic programming problem. In *2017 IEEE Congress on Evolutionary Computation (CEC)*, pages 557–564. IEEE, 2017.

[29] Kengo Katayama and Hiroyuki Narihisa. Performance of simulated annealing-based heuristic for the unconstrained binary quadratic programming problem. *European Journal of Operational Research*, 134(1):103–119, 2001.

[30] Arnaud Liefooghe, Sébastien Verel, Luis Paquete, and Jin-Kao Hao. Experiments on local search for bi-objective unconstrained binary quadratic programming. In *International Conference on Evolutionary Multi-Criterion Optimization*, pages 171–186. Springer, 2015.

[31] Murilo Zangari, Aurora Pozo, Roberto Santana, and Alexander Mendiburu. A decomposition-based binary aco algorithm for the multiobjective ubqp. *Neurocomputing*, 246(JUL.12):58–68, 2017.

[32] Zhipeng Lü, Jin-Kao Hao, and Fred Glover. A study of memetic search with multi-parent combination for ubqp. In *Evolutionary Computation in Combinatorial Optimization: 10th European Conference, EvoCOP 2010, Istanbul, Turkey, April 7-9, 2010. Proceedings 10*, pages 154–165. Springer, 2010.

[33] Yang Wang, Zhipeng Lü, Fred Glover, and Jin-Kao Hao. Probabilistic grasp-tabu search algorithms for the ubqp problem. *Computers and Operations Research*, 40:3100–3107, 12 2013.

[34] Yuan Jiang, Zhiguang Cao, and Jie Zhang. Learning to solve 3-d bin packing problem via deep reinforcement learning and constraint programming. *IEEE transactions on cybernetics*, 2021.

[35] Thomas Barrett, William Clements, Jakob Foerster, and Alex Lvovsky. Exploratory combinatorial optimization with reinforcement learning. In *Proceedings of the AAAI conference on artificial intelligence*, volume 34, pages 3243–3250, 2020.

[36] Irwan Bello, Hieu Pham, Quoc V Le, Mohammad Norouzi, and Samy Bengio. Neural combinatorial optimization with reinforcement learning. *International Conference on Learning Representations*, 2017.

[37] Wouter Kool, Herke van Hoof, and Max Welling. Attention, learn to solve routing problems! *International Conference on Learning Representations*, 2019.

[38] Yeong-Dae Kwon, Jinho Choo, Byoungjip Kim, Iljoo Yoon, Youngjune Gwon, and Seungjai Min. Pomo: Policy optimization with multiple optima for reinforcement learning. *Advances in Neural Information Processing Systems*, 33:21188–21198, 2020.

[39] Jieyi Bi, Yining Ma, Jiahai Wang, Zhiguang Cao, Jinbiao Chen, Yuan Sun, and Yeow Meng Chee. Learning generalizable models for vehicle routing problems via knowledge distillation. *Advances in Neural Information Processing Systems*, 35:31226–31238, 2022.

[40] Fu Luo, Xi Lin, Fei Liu, Qingfu Zhang, and Zhenkun Wang. Neural combinatorial optimization with heavy decoder: Toward large scale generalization. *Advances in Neural Information Processing Systems*, 36, 2024.

[41] Jinbiao Chen, Zizhen Zhang, Zhiguang Cao, Yaxin Wu, Yining Ma, Te Ye, and Jiahai Wang. Neural multi-objective combinatorial optimization with diversity enhancement. *Advances in Neural Information Processing Systems*, 36, 2024.

[42] Thomas N. Kipf and Max Welling. Semi-supervised classification with graph convolutional networks. In *International Conference on Learning Representations*, 2017.

[43] Qimai Li, Zhichao Han, and Xiao-Ming Wu. Deeper insights into graph convolutional networks for semi-supervised learning. In *Proceedings of the AAAI conference on artificial intelligence*, volume 32, 2018.

[44] D Kinga, Jimmy Ba Adam, et al. A method for stochastic optimization. In *International conference on learning representations (ICLR)*, volume 5, page 6. San Diego, California, 2015.

[45] John E Beasley. Obtaining test problems via internet. *Journal of Global Optimization*, 8:429–433, 1996.

[46] Gintaras Palubeckis. Multistart tabu search strategies for the unconstrained binary quadratic optimization problem. *Annals of Operations Research*, 131:259–282, 2004.

[47] Xavier Glorot and Yoshua Bengio. Understanding the difficulty of training deep feedforward neural networks. In *Proceedings of the thirteenth international conference on artificial intelligence and statistics*, pages 249–256. JMLR Workshop and Conference Proceedings, 2010.

- [48] LLC Gurobi Optimization. Gurobi optimizer reference manual, 2024.
- [49] Martin JA Schuetz, J Kyle Brubaker, and Helmut G Katzgraber. Combinatorial optimization with physics-inspired graph neural networks. *Nature Machine Intelligence*, 4(4):367–377, 2022.
- [50] Laurens Van der Maaten and Geoffrey Hinton. Visualizing data using t-sne. *Journal of machine learning research*, 9(11), 2008.
- [51] Ankur Nath and Alan Kuhnle. A benchmark for maximum cut: Towards standardization of the evaluation of learned heuristics for combinatorial optimization. *arXiv preprint arXiv:2406.11897*, 2024.

A The Neural Architecture within VCM

The overall neural architecture of solver VCM is plotted in Figure 9.

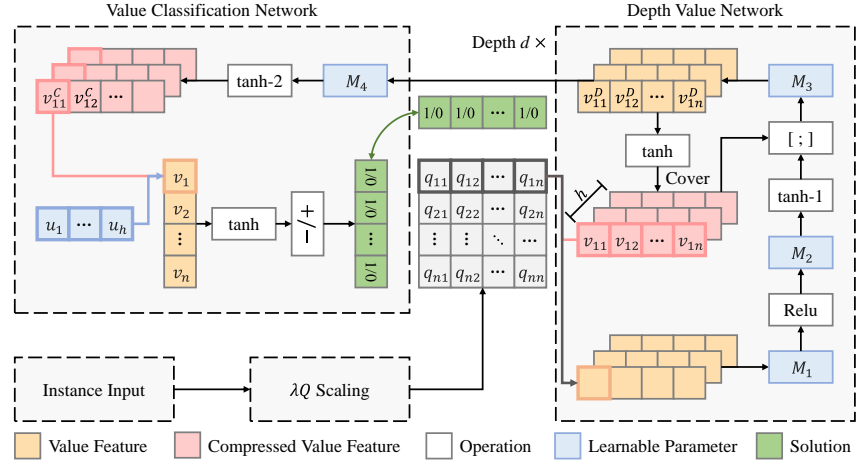


Figure 9: The neural architecture within VCM. The input Q is initially scaled by a scaling factor λ to improve value compression efficiency for the post-order Extractor DVN. Subsequently, DVN utilizes problem-tailored convolution to iteratively auto-grasp value features for each variable based on the specified iterative depth d and hidden size h . Finally, leveraging the acquired value features, the Classifier VCN generates the solution directly through a classification way.

Initially, in the Extractor DVN in VCM, the value feature V of tasks is denoted as V^0 with elements initialized to 1, so that all elements of the first QV^0 represent the sum of Q 's row rs . These values are significantly influenced by the instance size and dataset distribution, which may vary in magnitude. Therefore, preprocessing of the input data is crucial. To enhance value compression efficiency in DVN, we scale Q using a scaling function. For each Q , we take λQ to perform uniform scaling, where λ is the scaling factor calculated as:

$$s = \text{argmax}(\text{abs}(rs_1, rs_2, \dots, rs_n)) \quad (8)$$

$$\lambda = \alpha / (s + s_B) \quad (9)$$

Here, α is a handcrafted scaling constant, and s_B is the mean of s in each training batch. The proposed scaling function proves effective and plays a significant role in the performance of VCM (refer to the experimental results in Appendix F).

B Batch Calculation of Objective Function Increment

B.1 The Flip Operation

In the MDP for QUBO, the flip operation is fundamental, wherein a binary variable within the current solution transforms between 0 and 1 based on a specific strategy. The diagram of the flip operation is shown in Figure 10. The key basis for performing the flip operation is the calculation of the Objective Function Value Increment (OFI) after each variable is flipped, which is also an essential element of iterative search algorithms.

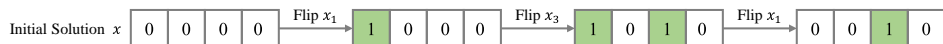


Figure 10: The flip operation in the MDP of QUBO.

B.2 Batch OFI Calculation Method

Traditional OFI computation, however, as depicted on the left side of Figure 11, suffers from inefficiency and resource wastage due to its instance-by-instance serial execution. To address the computational inefficiencies inherent in the traditional OFI computation and to accommodate batch instance requirements pivotal for the existing deep learning model, we propose an innovative batch OFI calculation method. As depicted on the right side of Figure 11, the batch OFI calculation allows for simultaneous OFI calculations across n variables in B instances.

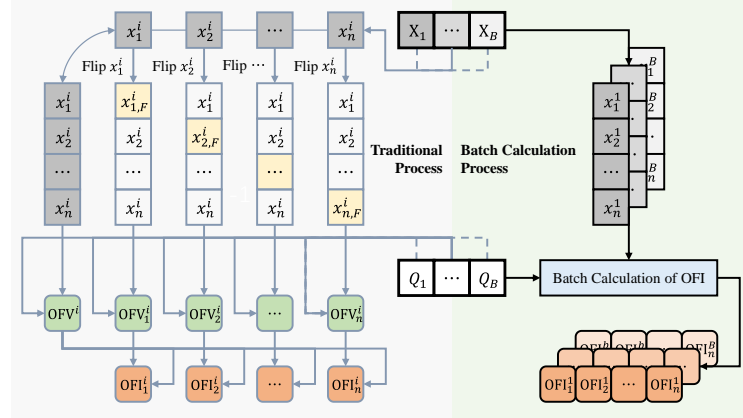


Figure 11: The OFI calculation process at each decision step of the traditional process and the proposed batch process in B instances. The traditional process entails a sequential, instance-by-instance approach in which the OFI for each variable x_i is serially and independently calculated at every decision step. In contrast, our proposed batch calculation process exploits the matrix computation to simplify and speed up the calculation process, enabling the determination of the OFI for n variables across batch B instances, with the potential for further acceleration through GPU.

We utilize matrix computation, presenting a detailed derivation process accordingly. We consider an $n \times n$ -dimensional symmetric QUBO matrix $Q = \{q_{ij}\}_{n \times n}$ where $q_{ij} = q_{ji}, i = 1..n, j = 1..n$.

$$Q = \begin{bmatrix} q_{11} & q_{12} & \dots & q_{1n} \\ q_{21} & q_{22} & & q_{2n} \\ \vdots & & \ddots & \vdots \\ q_{n1} & q_{n2} & \dots & q_{nn} \end{bmatrix} \quad (10)$$

The current QUBO solution $x = \{x_1, x_2, \dots, x_n\}$ is an n -dimensional vector. $N = \{1, 2, \dots, n\}$ indexes the elements of x and both the rows and columns of Q . Thus, Equation (1) is expanded as follows.

$$f(x) = \sum_{i=1}^n q_{ii} x_i^2 + \sum_{i=1}^n \sum_{j=1}^{i-1} q_{ij} x_i x_j + \sum_{i=1}^n \sum_{j=i+1}^n q_{ij} x_i x_j \quad (11)$$

We examine the effect of flipping the k -th variable on the solution, yielding a new solution x' in which x'_i is defined by:

$$x'_i = \begin{cases} 1 - x_i, & i = k \\ x_i, & i \neq k \end{cases} \quad (12)$$

The *OFV* for x' is then determined.

$$f(x') = \sum_{i=1}^n q_{ii} x'_i^2 + \sum_{i=1}^n \sum_{j=1}^{i-1} q_{ij} x'_i x'_j + \sum_{i=1}^n \sum_{j=i+1}^n q_{ij} x'_i x'_j \quad (13)$$

Subsequently, the OFI of the variable x_k is calculated as follows:

$$OFI(x_k) = f(x'_k) - f(x_k) = (x'_k - x_k) \\ \left[q_{kk} (x'_k + x_k) + \sum_{i \in N, i \neq k} q_{ik} x_i + \sum_{j \in N, j \neq k} q_{kj} x_j \right] \quad (14)$$

Because of $x'_k + x_k = 1$ and $q_{ij} = q_{ji}$, the function simplifies to:

$$OFI(x_k) = (x'_k - x_k) \left[q_{kk} + 2 \sum_{i \in N, i \neq k} q_{ik} x_i \right] \quad (15)$$

In this case, we define the sum of the k -th row Q_k^{sum} as follows:

$$Q_k^{sum} = \sum_{j \in N} q_{kj} x_j \quad (16)$$

All the Q^{sum} across all variables can be calculated as follows:

$$Q^{sum} = Q \cdot x \quad (17)$$

Then, the flip of $OFI(x_k)$ can be divided into two cases: 0 to 1 and 1 to 0. In the first case where $x_k = 0$ and $x'_k = 1$, the difference $x'_k - x_k = 1$, which modifies Equation (15) to:

$$OFI(x_k) = q_{kk} + 2 \sum_{j \in N, j \neq k} q_{kj} x_j \quad (18)$$

Since $x_k = 0$, we have $q_{kk} x_k = 0$, thereby expanding $OFI(x_k)$ as:

$$OFI(x_k) = q_{kk} + 2 \sum_{j \in N, j \neq k} q_{kj} x_j \\ = q_{kk} + 2 \sum_{j \in N, j \neq k} q_{kj} x_j + 2q_{kk} x_k \\ = q_{kk} + 2Q_k^{sum} \quad (19)$$

Conversely, when $x_k = 1$ and $x'_k = 0$, the difference $x'_k - x_k = -1$, adjusting Equation (15) to:

$$OFI(x_k) = -q_{kk} - 2 \sum_{j \in N, j \neq k} q_{kj} x_j \quad (20)$$

Because of $q_{kk} x_k = q_{kk}$ when $x_k = 1$. The $OFI(x_k)$ can be expanded as follows.

$$OFI(x_k) = -q_{kk} - 2 \sum_{j \in N, j \neq k} q_{kj} x_j \\ = q_{kk} - 2 \sum_{j \in N} q_{kj} x_j \\ = q_{kk} - 2Q_k^{sum} \quad (21)$$

Hence, the calculation of $OFI(x_k)$ can be concluded as follow:

$$OFI(x_k) = \begin{cases} q_{kk} + 2Q_k^{sum}, & x_k = 0 \\ q_{kk} - 2Q_k^{sum}, & x_k = 1 \end{cases} \quad (22)$$

Finially, we define the diagonal elements of the matrix Q as $Q^{diag} \in \mathbb{R}^{N \times 1}$ and propose the OFI batch calculation as follows:

$$OFI(x) = Q^{diag} + 2(1 - 2x)Q^{sum} \quad (23)$$

We evaluate the effectiveness of the proposed batch calculation of OFI using the following Greedy Flip method.

C Batch Greedy Flip Algorithm

During the MDP of QUBO, we execute the flip with the highest positive OFI at each state in a greedy manner to derive the Greedy Flip algorithm. In Figure 12, we provide a comprehensive illustration of the Greedy Flip algorithm's execution within a specific QUBO instance comprising four variables. Notably, variable x_1 undergoes two repeated flips.

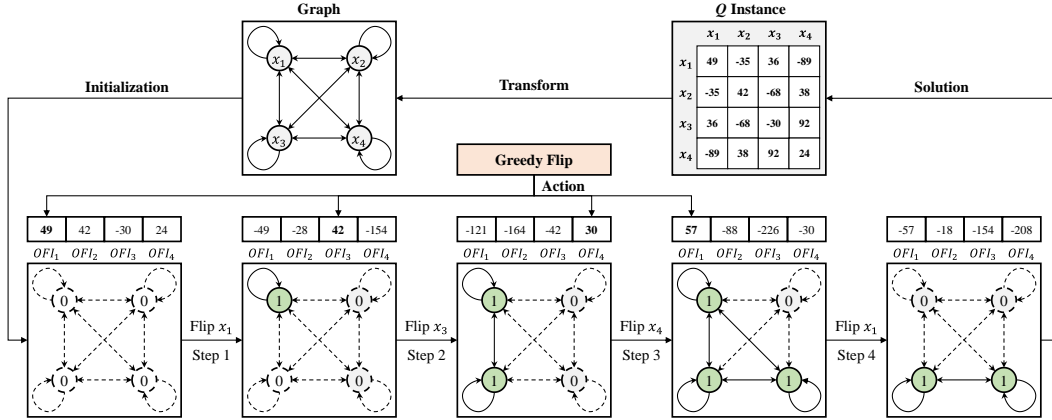


Figure 12: The Greedy Flip algorithm of QUBO.

Enhanced by the proposed OFI batch calculation method, we propose the Batch Greedy Flip (BGF) method for supporting the proposed GST. Besides, BGF is not only used as a competitor to validate the effectiveness of VCM but also as an enhancement component for VCM to integrate a powerful hybrid construction method VCM-BGF. The pseudo-code of BGF is presented in Algorithm 2. It is worth noting that the length of the solution for the batch calculation is $N + 1$, consisting of the problem solution with a set-aside point. In case the OFI of all variables in the current solution is non-positive OFI, the value of this set-aside point will be flipped.

Algorithm 2 The Batch Greedy Flip (BGF) algorithm

Input: the batch size B , the matrix of the batch $Q = \{Q_t | t = 1, \dots, B\}$, $Q_t \in \mathbb{R}^{(N+1) \times (N+1)}$, the initial solution of the batch $x = \{x_t | t = 1, \dots, B\}$, $x_t \in \mathbb{R}^{(N+1) \times 1}$

Output: the improved solution x^*

Calculate $Q^{diag} \in \mathbb{R}^{B \times (N+1) \times 1}$

while True **do**

$OFI_t \leftarrow Q_t^{diag} + 2(1 - 2x_t)Q_t^{sum}$

if $\forall OFI_{ti} \leq 0$, $t = \{1, \dots, B\}$, $i = \{1, \dots, N\}$ **then**

break

else

for $t = 1$ **to** B **do**

if $\forall OFI_{ti} \leq 0$, $i = \{1, \dots, N\}$ **then**

$k \leftarrow N + 1$

else

$k \leftarrow \arg \max_{k \in \{1, \dots, N\}} OFI_{tk}$

end if

$x_{tk} = 1 - x_{tk}$

end for

end if

end while

C.1 The Efficiency of Batch Calculation

To investigate the effectiveness of the proposed OFI batch calculation, we conduct tests on 1,000 generated G instances with 20, 50, 100, 200, 500, and 1,000 variables, using BGF with batch sizes of 1, 32, 64, 128, and 256. For comparative validation, we apply the Traditional Greedy Flip (TGF) method as the competitor, which calculates the OFI in a sequential and instance-by-instance way. We plot the running time curve in Figure 13 and detail the data in Table 2. The results reveal that the OFI batch calculation can significantly enhance the computing efficiency of the Greedy Flip method, which brings orders of magnitude efficiency improvement. With a batch size of 1, BGF-01 operates similarly to TGF, calculating instance by instance, where the difference between these two methods lies in the OFI calculation process of all variables in each decision step. Based on the batch calculation, BGF distinguishes itself by calculating the OFI for all variables simultaneously within a single step, as opposed to the sequential approach of TGF. This capability affords BGF a marked efficiency edge which grows with problem size, exemplified by its requirement of only 0.696% of the traditional calculation time for G1000 instances. The efficiency gains from OFI batch calculation are even more pronounced when dealing with batch instance computing. This improvement stems from the lower computational complexity afforded by the matrix computation process and the GPU acceleration. Consequently, the proposed OFI batch calculation method represents a potent computational tool for QUBO research, with promising applications beyond the scope of this work to potentially expedite a broad range of existing QUBO methods.

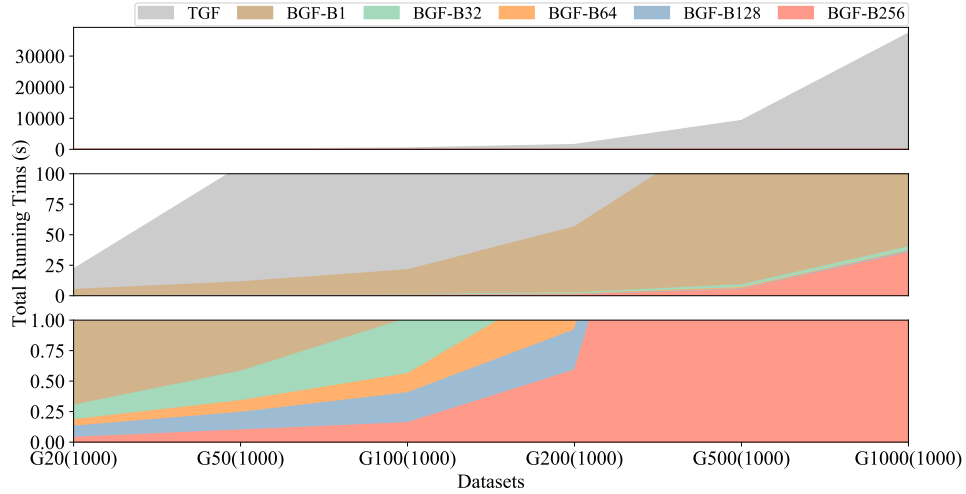


Figure 13: Total running time (s) of TGF and BGFs in different instances.

Table 2: Total running time of TGF and BGFs in different instances.

INSTANCE	TGF	BGF-B1	BGF-B32	BGF-B64	BGF-B128	BGF-B256
	TIME (S)					
G20(1000)	21.92	5.01	0.30	0.18	0.13	0.04
G50(1000)	106.08	11.34	0.58	0.34	0.24	0.10
G100(1000)	428.49	21.20	1.02	0.56	0.40	0.16
G200(1000)	1549.55	56.41	2.38	1.37	0.92	0.59
G500(1000)	9283.51	144.51	8.94	6.62	5.66	5.10
G1000(1000)	37365.85	260.12	40.04	36.87	36.42	35.32

C.2 BGF with Different Initial Solution

To investigate the effect of the initial solution on the BGF, we apply various initial solutions with different percentages of 1, including 0, 25%, 50%, 75%, and 100%. We set the test batch size to 256 and take the generated instances for testing, including G20(1000), G50(1000), G100(1000),

G200(1000), G500(1000), and G1000(1000). Except for 0 and 100%, all BGFs are run ten times on average. The results of average *OFV* and total running time are shown in Table 3, where we can find that the BGF with 100% of 1 outperforms all other test sizes in terms of both quality and speed. Therefore, we take the BGF-100% as the default BGF.

Table 3: Average *OFV* and total running time of BGF with different initial solutions.

INSTANCE	BGF-0		BGF-25%		BGF-50%		BGF-75%		BGF-100%	
	<i>OFV</i>	TIME (S)	<i>OFV</i>	TIME (S)						
G20(1000)	2838	0.09	2841	0.06	2859	0.05	2888	0.05	2916	0.04
G50(1000)	11659	0.18	11687	0.13	11736	0.12	11800	0.11	11901	0.10
G100(1000)	33381	0.34	33460	0.27	33522	0.26	33679	0.22	33892	0.16
G200(1000)	94907	1.21	95036	1.04	95251	0.91	95556	0.76	96022	0.59
G500(1000)	379096	11.75	379624	9.74	380133	8.16	380816	6.65	382412	5.10
G1000(1000)	1075398	88.50	1076710	71.81	1077693	59.09	1079293	48.13	1082420	35.32

D Wilcoxon Signed-rank Tests

We perform Wilcoxon signed-rank tests on the gap results obtained from the trained VCMs in comparison to other algorithms across 31 instances from the B and P sets. The results are summarized in Table 4, which clearly show significant differences between the VCM results and those of other algorithms, with the highest P-value being 3.09E-03 between VCM100 and BGF.

Table 4: The P-value results of Wilcoxon signed-rank test between VCMs and other algorithms.

ALGORITHM	VCM10	VCM20	VCM50	VCM100
DIAG	1.17E-06	1.30E-06	4.53E-06	4.97E-06
SR	1.77E-05	1.43E-06	5.46E-06	2.56E-06
BGF	1.17E-06	1.94E-05	2.12E-04	3.09E-03
DRLH-B	1.17E-06	1.17E-06	1.17E-06	1.17E-06
S2V-DQN-B	3.79E-06	3.79E-06	4.23E-06	3.79E-06
ECO-DQN-B	3.79E-06	3.79E-06	3.79E-06	3.79E-06
VCM10-BGF	1.17E-06	1.17E-06	1.30E-06	2.56E-06
VCM20-BGF	2.56E-06	1.17E-06	2.56E-06	1.43E-06
VCM50-BGF	1.17E-06	1.17E-06	1.17E-06	1.17E-06
VCM100-BGF	1.74E-06	1.17E-06	1.74E-06	1.17E-06
PI-GNN(2-LAYER)	1.17E-06	1.17E-06	1.17E-06	1.17E-06
PI-GNN(3-LAYER)	1.17E-06	1.17E-06	1.17E-06	1.17E-06
PI-GNN(5-LAYER)	1.17E-06	1.17E-06	1.17E-06	1.17E-06
GUROBI-1s	1.17E-06	1.17E-06	1.17E-06	1.17E-06
GUROBI-1h	1.17E-06	1.17E-06	1.17E-06	1.17E-06
VCM-BGF-HB	2.52E-05	1.30E-06	1.30E-06	1.17E-06

E Ablation Study

To validate the rationally designed network architecture of our VCM, we test the training performance of VCM by selectively ablating specific modules. We employ the VCM-() with the ablation module to distinguish different VCMs. Specifically, we select the VCM-(ReLU), VCM-(tanh1), VCM-(tanh2), VCM-(M1) and VCM-(M2) for validation. The ablation module can be quickly queried in Figure 9. The corresponding impacts of these ablations are captured in Figure 14, illustrating that any deficient module degrades VCM performance, notably ReLU and tanh2 modules. ReLU is pivotal for extracting value features, while tanh2 normalizes value features within a range of (-1, 1), essential for the unification of DVN extraction.

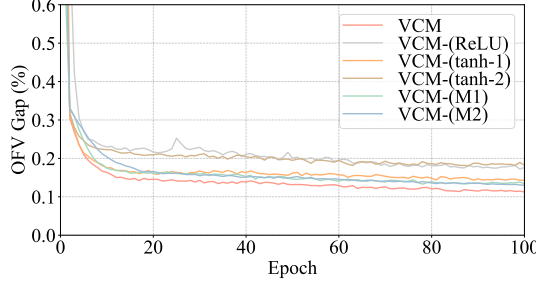


Figure 14: The VCM training process of ablation study at instance size 50.

F Parameter Study

F.1 The Scaling Parameter α

We train the VCM with α of 2, 4 (default), 6, and None (without scaling function) at instance size 50. The training process is shown in Figure 15, where we observe that the α can improve the performance of the VCM. Notably, the default VCM ($\alpha = 4$) achieves most of the training lead. We believe the scaling function of data compression makes tanh-1 more sensitive to input processing in the early stages. According to Equation (9), the optimal $\alpha = 4$ can compress the first input value (sum of each row) of DVN to an average of about 2, regardless of instance size and dataset distribution. It should be noted that when the input value exceeds 2, there is a negligible difference in the output by tanh. Therefore, using tanh-1 in the first depth of the default VCM can better compress and distinguish features, thereby accelerating model learning.

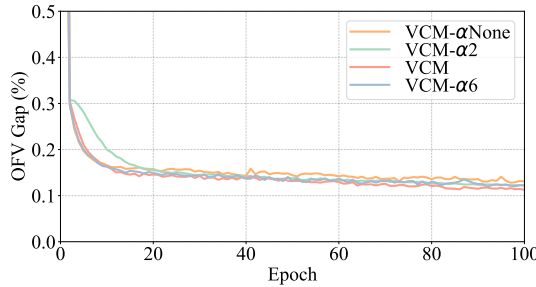


Figure 15: Training process of VCM with different α at instance size 50.

F.2 The DVN Depth d

A certain depth of DVN extraction is mandatory for ensuring interaction and coherence between the row and column features. To assess the impact of varying depths d on the performance of VCM, we set the training d of VCM50 to 10, 20, 30, 40 (default), 50, and 100 within an instance size of 50 for validation. As depicted in Figure 16 in Appendix E, the training trajectories of these six VCMs demonstrate that increasing depth (within our test range) enhances feature extraction precision, yielding a consistent improvement in VCM performance. Notably, the performance gain is pronounced as the depth extends from 10 to 30, but it plateaus thereafter. This trend suggests that a certain threshold of DVN depth is required to accomplish thorough value feature extraction from Q . While deeper d can enhance performance, the training costs also incur greater. Therefore, we elected to set d at the most cost-efficient value of 40 by default.

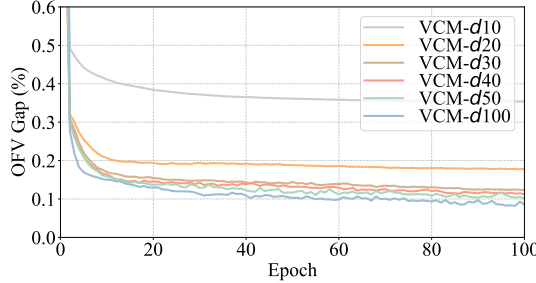


Figure 16: Training process of VCM with DVN depth d at instance size 50.

E.3 The Value Feature Size h

To evaluate the impact of h on VCM performance, we train the model with various values of $h = 32, 64, 128$ (default), and 256 for an instance size of 50 . As shown in Figure 17, the results indicate a significant improvement in VCM performance with the increase of h . Notably, the default setting of $h = 128$ achieves the highest training advancement, indicating that increasing the value feature size within a reasonable range enhances model performance effectively.

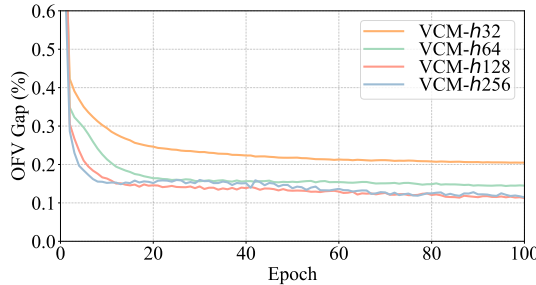


Figure 17: Training process of VCM with value feature size h at instance size 50.

G Results of Size Generalization

This section details the results of the size generation experiment. We conduct tests on an additional 1,000 generated G instances with 20, 50, 100, 200, 500, and 1,000 variables. The VCM-BGF-HB is applied as the current optimal baseline for gap calculation. The detailed results are depicted in Table 5. Notably, Gurobi incurs a significant time cost, and the results for G set with over 100 variables are omitted as each instance takes more than 1 hour.

H Results of Distribution Generalization

This section details the results of the distribution generation experiment in the Model Study. We conduct tests with five different distributions on these G instances with 20, 50, and 100 variables using our trained corresponding-sized VCMs, including the standard normal random (RN-1) and the uniform random with probabilities of 0 for 10% (R-0.1), 30% (R-0.3), 60% (R-0.6), 90% (R-0.9). For each test dataset, we generate 1,000 G instances and also apply VCM-BGF-HB as the current optimal baseline to measure the gap. The results are detailed in Table 6, with heatmaps provided in Figure 18.

Table 5: Results on generated datasets.

METHOD	G20(1000)		G50(1000)		G100(1000)		G200(1000)		G500(1000)		G1000(1000)	
	OBJECTIVE FUNCTION VALUE BASELINE											
	2965.095		12070.455		34350.38		97260.38		386638.40		1093972.99	
	GAP (%)	ART (ms)	GAP (%)	ART (ms)	GAP (%)	ART (ms)	GAP (%)	ART (ms)	GAP (%)	ART (ms)	GAP (%)	ART (ms)
DIAG	84.098	0.1	90.229	0.1	92.569	0.1	94.882	0.2	96.561	0.4	97.632	0.9
SR	31.637	3.5E-02	32.594	3.9E-02	32.628	3.5E-02	33.189	4.5E-02	32.915	4.6E-02	33.054	4.6E-02
VCM10	0.060	4.4	0.108	4.4	0.151	4.8	0.248	7.4	0.338	7.4	0.414	7.5
VCM20	0.121	4.4	0.112	4.7	0.196	4.7	0.257	7.3	0.409	7.4	0.507	7.5
VCM50	0.200	4.4	0.129	4.4	0.167	4.8	0.230	7.3	0.382	7.4	0.523	7.5
VCM100	0.244	4.4	0.117	4.4	0.207	4.8	0.207	7.3	0.357	7.4	0.508	7.5
BGF	1.642	5.2	1.401	11.7	1.335	23.1	1.273	60.8	1.093	158.1	1.056	294.2
DRLH-B	2.034	8.4	1.871	17.8	1.848	34.3	1.926	91.5	1.930	220.4	1.914	397.3
ECO-DQN-B	0.321	43.2	0.362	109.5	0.471	216.6	0.731	636.2	1.004	2.3E+03	1.160	1.3E+04
S2V-DQN-B	4.007	22.9	4.966	57.1	5.758	115.0	6.414	338.5	7.173	1.2E+03	7.567	6.4E+03
VCM10-BGF	0.025	5.1	0.058	5.2	0.089	5.7	0.148	9.3	0.209	11.6	0.258	16.5
VCM20-BGF	0.010	5.1	0.037	5.5	0.066	5.7	0.107	9.3	0.173	12.6	0.223	18.8
VCM50-BGF	0.036	5.1	0.019	5.2	0.044	5.7	0.064	9.3	0.113	12.4	0.163	19.6
VCM100-BGF	0.052	5.1	0.027	5.1	0.042	5.7	0.050	9.2	0.094	12.3	0.138	19.6
GUROBI	0*	54.3	0*	3.7E+03	-	>1H	-	-	-	-	-	-
VCM-BGF-HB	0.0003	509.1	0.0005	526.0	0*	572.3	0*	926.6	0*	1.2E+03	0*	1.9E+03

¹ The **Bold** indicates the best average result in different classes of methods.

² The * indicates the provider of the applied *OFV* baseline.

Table 6: Distribution generalization results on generated datasets.

SIZE	INSTANCE	G-RN-1			G-R-0.1			G-R-0.3			G-R-0.6			G-R-0.9		
		OFV	GAP (%)	ART (ms)												
20	BGF	5089.9	1.34	5.9	793.9	1.32	3.7	1560.5	1.74	4.7	2234.4	1.55	4.7	2770.7	1.49	4.8
	VCM	5154.2	0.09	4.7	803.4	0.14	4.4	1586.8	0.08	4.4	2266.6	0.13	4.4	2809.2	0.12	4.3
	VCM-BGF	5157.8	0.02	5.4	804.4	0.02	5.1	1587.9	0.01	5.1	2269.0	0.02	5.1	2811.9	0.02	5.1
50	VCM-BGF-HB	5158.9*	-	2.2E+03	804.5*	-	2.0E+03	1588.1*	-	2.0E+03	2269.5*	-	2.0E+03	2812.5*	-	2.0E+03
	BGF	20457.5	1.40	12.3	3557.7	1.64	10.1	6392.9	1.64	10.6	9121.7	1.51	10.8	11280.1	1.36	11.1
	VCM	20724.8	0.11	4.6	3611.1	0.17	4.4	6495.0	0.07	4.4	9247.4	0.15	4.4	11421.5	0.12	4.4
100	VCM-BGF	20743.0	0.02	5.5	3616.2	0.02	5.2	6498.4	0.02	5.1	9259.3	0.03	5.1	11433.4	0.02	5.1
	VCM-BGF-HB	20747.9*	-	2.2E+03	3617.1*	-	2.1E+03	6499.8*	-	2.0E+03	9261.6*	-	2.1E+03	11435.5*	-	2.1E+03
	BGF	58031.7	1.38	23.3	10505.5	1.64	20.7	18462.2	1.48	24.4	26199.1	1.47	20.9	32279.1	1.27	22.4
	VCM	58756.3	0.15	5.0	10664.7	0.15	4.8	18713.0	0.14	4.8	26556.2	0.13	5.2	32641.2	0.16	4.7
	VCM-BGF	58824.2	0.04	6.0	10676.8	0.04	5.6	18732.2	0.04	5.7	26584.1	0.03	6.2	32683.1	0.03	5.7
	VCM-BGF-HB	58844.9*	-	2.4E+03	10680.6*	-	2.2E+03	18739.1*	-	2.3E+03	26591.2*	-	2.5E+03	32693.5*	-	2.3E+03

¹ The **Bold** indicates the best average result in different datasets.

² The * indicates the provider of the applied *OFV* baseline.

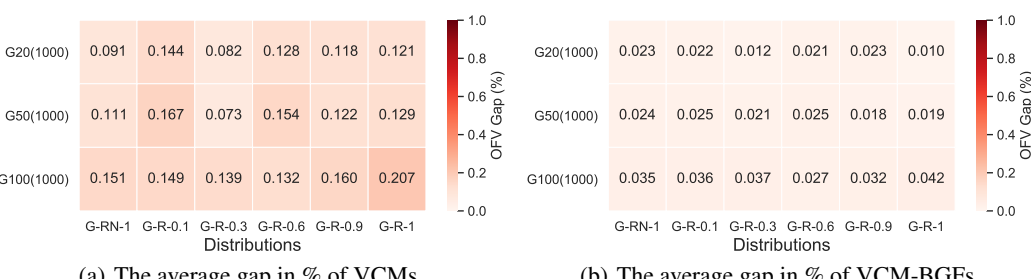


Figure 18: Heatmaps of distribution generalization obtained by VCMs under G-R-1 with corresponding instance size.

I Results of MaxCut Benchmarks

We extend our evaluation to MaxCut benchmarks, with the results presented below. Utilizing data from [15], we compile the results shown in Table 7, using the average objective function value as

the key indicator. Additionally, based on data from [51], we present the results in Table 8, where the average approximation ratios serve as the performance indicator.

The results confirm that VCM outperforms other methods, consistent with the advantages demonstrated in our test instances. This validates the applicability and robustness of our VCM in problems that can be recasted as QUBO across different scales and distributions.

Table 7: Results on MaxCut benchmarks.

INSTANCE	OPT	S2V-DQN	VCM50-d100
G54100-G5410000 (10 INSTANCES)	110.6	108.2	109.6(5MS)

Table 8: Results on large MaxCut benchmarks.

INSTANCE	TABU	SOFTTABU	S2V-DQN	ECO-DQN	VCM-d100	VCM-BGF-d100
G32-G34 (2000 NODES)	0.915	0.983	0.923	0.969	0.990(16MS)	0.991(23MS)

J Results of DVN depths

This section details the results of the DVN depth experiment in the Model Study. We train VCM50s across various depths d including 10, 20, 30, 40, 50, and 100. Each trained specific-size VCM is tested across an extended range of depths, including 10, 20, 30, 40, 50, 100, 200, and 300. The average gap (GAP) and average running time (ART) on benchmarks B2500(10) are listed in Table 9. The corresponding heatmap is illustrated in Figure 19.

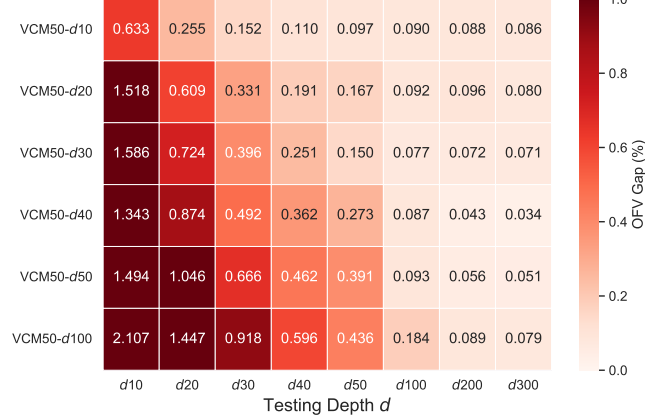


Figure 19: Heatmaps of test depths under VCM50 models with different training depths d .

Table 9: Results of DVN depths on benchmarks B2500(10).

METHOD	10		20		30		40		50		100		200		300	
	GAP (%)	ART (MS)	GAP (%)	ART (MS)												
VCM50-d10	0.633	2.6	0.255	4.4	0.152	6.1	0.110	7.8	0.097	9.6	0.090	18.2	0.088	35.5	0.086	53.1
VCM50-d20	1.518	2.6	0.609	4.4	0.331	6.0	0.191	7.8	0.167	9.6	0.092	18.3	0.096	35.5	0.080	53.2
VCM50-d30	1.586	2.6	0.724	4.3	0.396	6.1	0.251	7.8	0.150	9.6	0.077	18.3	0.072	35.5	0.071	53.2
VCM50-d40	1.343	2.6	0.874	4.4	0.492	6.1	0.362	7.8	0.273	9.6	0.087	18.3	0.043	35.5	0.034	52.8
VCM50-d50	1.494	2.6	1.046	4.3	0.666	6.1	0.462	7.8	0.391	9.5	0.093	18.4	0.056	35.5	0.051	52.8
VCM50-d100	2.107	2.6	1.447	4.3	0.918	6.1	0.596	7.8	0.436	9.6	0.184	18.6	0.089	35.5	0.079	52.8

In addition, we evaluate the VCM50 and VCM50-BGF at the default testing depth of $d = 40$ and a deeper depth of $d = 300$. The results on benchmarks and large well-known instances are presented in Table 10. We use Gurobi-1s as the baseline for comparison.

Table 10: Results on benchmarks and large well-known instances.

ALGORITHM	B2500(10)	P3000(5)	P4000(5)	P5000(5)	P6000(3)	P7000(3)						
	OBJECTIVE FUNCTION VALUE BASELINE (OPTIMAL)											
	1479921.4	5134727.2	7869134.2	10973791.4	13950582.0	17725010.33						
	GAP (%)	ART (ms)	GAP (%)	ART (ms)	GAP (%)	ART (ms)	GAP (%)	ART (ms)	GAP (%)	ART (ms)		
GUROBI-1s	0.034	1.0E+03	0.070	1.0E+03	0.108	1.0E+03	0.091	1.0E+03	0.122	1.0E+03	0.145	1.0E+03
VCM50	0.362	8	0.861	8	0.669	8	0.783	8	0.806	9	0.702	9
VCM50-d300	0.034	52	0.066	53	0.115	52	0.099	53	0.144	76	0.144	116
VCM50-BGF	0.136	44	0.277	100	0.214	170	0.262	326	0.267	523	0.224	770
VCM50-d300-BGF	0.027	64	0.04	79	0.088	108	0.078	145	0.109	249	0.108	331

K Results of Degradation in GCN

We apply GCN [42] to replace the DVN in VCM and confirm performance degradation with increased layers, consistent with [42]. We train GCN and VCM by GST on size 50 under the same settings. The training details are shown in Figure 20 and the optimal training gaps are shown in Figure 21.

Obviously, the GCN suffers from performance degradation, which is consistent with the conclusion in [42]. However, the performance of VCM steadily improves with increasing depth. Besides, the neural parameters in GCN layers are independent, whereas neural units in VCM depth are consistent, resulting in lower training costs under the same neural settings.

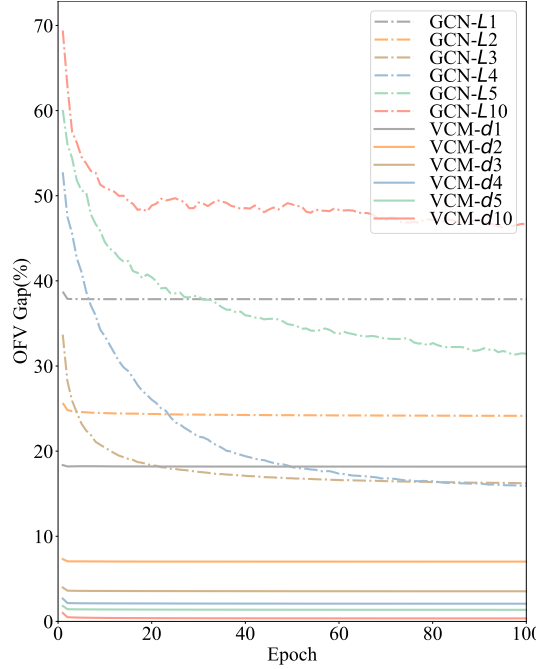


Figure 20: The training processes of GCN and VCM under different training layer L or depth d at instance size 50.

L Results of Very Large Instances

This section presents the results obtained from testing very large instances. We conduct experiments on a single generated G instance with sizes of 10,000 and 20,000, using distributions R-0.1 and R-0.3.

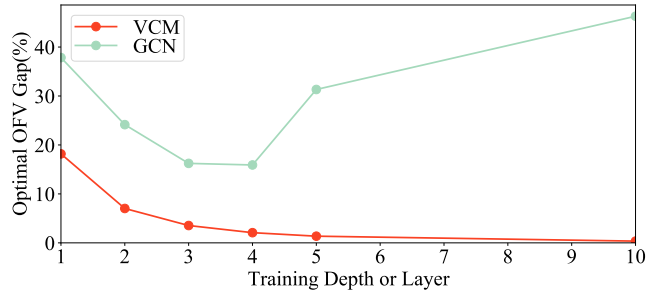


Figure 21: The optimal training OFV gap of GCN and VCM under different training layer L or depth d at instance size 50.

The model VCM50- d 300 is evaluated against Gurobi, which served as the baseline with a maximum allowable runtime of 1 second, referred to as Gurobi-1s.

To assess performance, we utilize the OFV gap between Gurobi-1s and VCM50- d 300 as the metric. The results are summarized in Table 11. Notably, VCM50- d 300 consistently outperforms Gurobi-1s in terms of both solution quality and execution speed, demonstrating its effectiveness on very large instances across various distributions.

Table 11: Results on generated large size instances.

METHOD	G10000-R0.1(1)		G10000-R0.3(1)		G20000-R0.1(1)		G20000-R0.3(1)	
	GAP (%)	T (ms)						
GUROBI-1s	0.183	1.0E+03	0.045	1.0E+03	0.091	1.0E+03	0.108	1.0E+03
VCM50- d 300	0	169	0	172	0	637	0	676

NeurIPS Paper Checklist

1. Claims

Question: Do the main claims made in the abstract and introduction accurately reflect the paper's contributions and scope?

Answer: **[Yes]**

Justification: In the abstract and introduction, we have provided a detailed and accurate description of the scope of the research, related works in QUBO, limitations of current research on learning-based models, and the contributions of this paper.

Guidelines:

- The answer NA means that the abstract and introduction do not include the claims made in the paper.
- The abstract and/or introduction should clearly state the claims made, including the contributions made in the paper and important assumptions and limitations. A No or NA answer to this question will not be perceived well by the reviewers.
- The claims made should match theoretical and experimental results, and reflect how much the results can be expected to generalize to other settings.
- It is fine to include aspirational goals as motivation as long as it is clear that these goals are not attained by the paper.

2. Limitations

Question: Does the paper discuss the limitations of the work performed by the authors?

Answer: **[Yes]**

Justification: We have discussed the limitations of our neural solver VCM in the Section 5, Conclusion and Future Work. The optimality of VCM may be potentially limited by the utilization of value features from the Extractor DVN by the Classifier VCN.

Guidelines:

- The answer NA means that the paper has no limitation while the answer No means that the paper has limitations, but those are not discussed in the paper.
- The authors are encouraged to create a separate "Limitations" section in their paper.
- The paper should point out any strong assumptions and how robust the results are to violations of these assumptions (e.g., independence assumptions, noiseless settings, model well-specification, asymptotic approximations only holding locally). The authors should reflect on how these assumptions might be violated in practice and what the implications would be.
- The authors should reflect on the scope of the claims made, e.g., if the approach was only tested on a few datasets or with a few runs. In general, empirical results often depend on implicit assumptions, which should be articulated.
- The authors should reflect on the factors that influence the performance of the approach. For example, a facial recognition algorithm may perform poorly when image resolution is low or images are taken in low lighting. Or a speech-to-text system might not be used reliably to provide closed captions for online lectures because it fails to handle technical jargon.
- The authors should discuss the computational efficiency of the proposed algorithms and how they scale with dataset size.
- If applicable, the authors should discuss possible limitations of their approach to address problems of privacy and fairness.
- While the authors might fear that complete honesty about limitations might be used by reviewers as grounds for rejection, a worse outcome might be that reviewers discover limitations that aren't acknowledged in the paper. The authors should use their best judgment and recognize that individual actions in favor of transparency play an important role in developing norms that preserve the integrity of the community. Reviewers will be specifically instructed to not penalize honesty concerning limitations.

3. Theory Assumptions and Proofs

Question: For each theoretical result, does the paper provide the full set of assumptions and a complete (and correct) proof?

Answer: [Yes]

Justification: We have provided the full set of assumptions and a complete (and correct) proof in Section 3 and Appendix B. We detailed the proposed neural solver VCM in Section 3 and the derivation procedure of the proposed Batch Calculation of Objective Function Increment (OFI).

Guidelines:

- The answer NA means that the paper does not include theoretical results.
- All the theorems, formulas, and proofs in the paper should be numbered and cross-referenced.
- All assumptions should be clearly stated or referenced in the statement of any theorems.
- The proofs can either appear in the main paper or the supplemental material, but if they appear in the supplemental material, the authors are encouraged to provide a short proof sketch to provide intuition.
- Inversely, any informal proof provided in the core of the paper should be complemented by formal proofs provided in appendix or supplemental material.
- Theorems and Lemmas that the proof relies upon should be properly referenced.

4. Experimental Result Reproducibility

Question: Does the paper fully disclose all the information needed to reproduce the main experimental results of the paper to the extent that it affects the main claims and/or conclusions of the paper (regardless of whether the code and data are provided or not)?

Answer: [Yes]

Justification: We have fully disclosed all the information needed to reproduce the main experimental results of the paper to the extent, including the neural architecture, hyperparameters of our VCM, and the dataset generation format.

Guidelines:

- The answer NA means that the paper does not include experiments.
- If the paper includes experiments, a No answer to this question will not be perceived well by the reviewers: Making the paper reproducible is important, regardless of whether the code and data are provided or not.
- If the contribution is a dataset and/or model, the authors should describe the steps taken to make their results reproducible or verifiable.
- Depending on the contribution, reproducibility can be accomplished in various ways. For example, if the contribution is a novel architecture, describing the architecture fully might suffice, or if the contribution is a specific model and empirical evaluation, it may be necessary to either make it possible for others to replicate the model with the same dataset, or provide access to the model. In general, releasing code and data is often one good way to accomplish this, but reproducibility can also be provided via detailed instructions for how to replicate the results, access to a hosted model (e.g., in the case of a large language model), releasing of a model checkpoint, or other means that are appropriate to the research performed.
- While NeurIPS does not require releasing code, the conference does require all submissions to provide some reasonable avenue for reproducibility, which may depend on the nature of the contribution. For example
 - (a) If the contribution is primarily a new algorithm, the paper should make it clear how to reproduce that algorithm.
 - (b) If the contribution is primarily a new model architecture, the paper should describe the architecture clearly and fully.
 - (c) If the contribution is a new model (e.g., a large language model), then there should either be a way to access this model for reproducing the results or a way to reproduce the model (e.g., with an open-source dataset or instructions for how to construct the dataset).

(d) We recognize that reproducibility may be tricky in some cases, in which case authors are welcome to describe the particular way they provide for reproducibility. In the case of closed-source models, it may be that access to the model is limited in some way (e.g., to registered users), but it should be possible for other researchers to have some path to reproducing or verifying the results.

5. Open access to data and code

Question: Does the paper provide open access to the data and code, with sufficient instructions to faithfully reproduce the main experimental results, as described in supplemental material?

Answer: **[No]**

Justification: If the paper is accepted, the data and code will be considered for public release.

Guidelines:

- The answer NA means that paper does not include experiments requiring code.
- Please see the NeurIPS code and data submission guidelines (<https://nips.cc/public/guides/CodeSubmissionPolicy>) for more details.
- While we encourage the release of code and data, we understand that this might not be possible, so “No” is an acceptable answer. Papers cannot be rejected simply for not including code, unless this is central to the contribution (e.g., for a new open-source benchmark).
- The instructions should contain the exact command and environment needed to run to reproduce the results. See the NeurIPS code and data submission guidelines (<https://nips.cc/public/guides/CodeSubmissionPolicy>) for more details.
- The authors should provide instructions on data access and preparation, including how to access the raw data, preprocessed data, intermediate data, and generated data, etc.
- The authors should provide scripts to reproduce all experimental results for the new proposed method and baselines. If only a subset of experiments are reproducible, they should state which ones are omitted from the script and why.
- At submission time, to preserve anonymity, the authors should release anonymized versions (if applicable).
- Providing as much information as possible in supplemental material (appended to the paper) is recommended, but including URLs to data and code is permitted.

6. Experimental Setting/Details

Question: Does the paper specify all the training and test details (e.g., data splits, hyper-parameters, how they were chosen, type of optimizer, etc.) necessary to understand the results?

Answer: **[Yes]**

Justification: We have specified all the training and test detail in Section 4.1, Experimental Details.

Guidelines:

- The answer NA means that the paper does not include experiments.
- The experimental setting should be presented in the core of the paper to a level of detail that is necessary to appreciate the results and make sense of them.
- The full details can be provided either with the code, in appendix, or as supplemental material.

7. Experiment Statistical Significance

Question: Does the paper report error bars suitably and correctly defined or other appropriate information about the statistical significance of the experiments?

Answer: **[Yes]**

Justification: We have performed Wilcoxon signed-rank tests and detailed the results in Appendix D.

Guidelines:

- The answer NA means that the paper does not include experiments.
- The authors should answer "Yes" if the results are accompanied by error bars, confidence intervals, or statistical significance tests, at least for the experiments that support the main claims of the paper.
- The factors of variability that the error bars are capturing should be clearly stated (for example, train/test split, initialization, random drawing of some parameter, or overall run with given experimental conditions).
- The method for calculating the error bars should be explained (closed form formula, call to a library function, bootstrap, etc.)
- The assumptions made should be given (e.g., Normally distributed errors).
- It should be clear whether the error bar is the standard deviation or the standard error of the mean.
- It is OK to report 1-sigma error bars, but one should state it. The authors should preferably report a 2-sigma error bar than state that they have a 96% CI, if the hypothesis of Normality of errors is not verified.
- For asymmetric distributions, the authors should be careful not to show in tables or figures symmetric error bars that would yield results that are out of range (e.g. negative error rates).
- If error bars are reported in tables or plots, The authors should explain in the text how they were calculated and reference the corresponding figures or tables in the text.

8. Experiments Compute Resources

Question: For each experiment, does the paper provide sufficient information on the computer resources (type of compute workers, memory, time of execution) needed to reproduce the experiments?

Answer: [\[Yes\]](#)

Justification: We have provided sufficient information on the computer resources in Section 4.1, Experimental Details, specifically in the subsection on Hyperparameters.

Guidelines:

- The answer NA means that the paper does not include experiments.
- The paper should indicate the type of compute workers CPU or GPU, internal cluster, or cloud provider, including relevant memory and storage.
- The paper should provide the amount of compute required for each of the individual experimental runs as well as estimate the total compute.
- The paper should disclose whether the full research project required more compute than the experiments reported in the paper (e.g., preliminary or failed experiments that didn't make it into the paper).

9. Code Of Ethics

Question: Does the research conducted in the paper conform, in every respect, with the NeurIPS Code of Ethics <https://neurips.cc/public/EthicsGuidelines>?

Answer: [\[Yes\]](#)

Justification: The research conducted in the paper conform, in every respect, with the NeurIPS Code of Ethics.

Guidelines:

- The answer NA means that the authors have not reviewed the NeurIPS Code of Ethics.
- If the authors answer No, they should explain the special circumstances that require a deviation from the Code of Ethics.
- The authors should make sure to preserve anonymity (e.g., if there is a special consideration due to laws or regulations in their jurisdiction).

10. Broader Impacts

Question: Does the paper discuss both potential positive societal impacts and negative societal impacts of the work performed?

Answer: [\[Yes\]](#)

Justification: We have discussed the potential impacts of the work performed in the Section 1, Introduction. The QUBO studied in this work is able to represent a remarkable spectrum of applications in combinatorial optimization.

Guidelines:

- The answer NA means that there is no societal impact of the work performed.
- If the authors answer NA or No, they should explain why their work has no societal impact or why the paper does not address societal impact.
- Examples of negative societal impacts include potential malicious or unintended uses (e.g., disinformation, generating fake profiles, surveillance), fairness considerations (e.g., deployment of technologies that could make decisions that unfairly impact specific groups), privacy considerations, and security considerations.
- The conference expects that many papers will be foundational research and not tied to particular applications, let alone deployments. However, if there is a direct path to any negative applications, the authors should point it out. For example, it is legitimate to point out that an improvement in the quality of generative models could be used to generate deepfakes for disinformation. On the other hand, it is not needed to point out that a generic algorithm for optimizing neural networks could enable people to train models that generate Deepfakes faster.
- The authors should consider possible harms that could arise when the technology is being used as intended and functioning correctly, harms that could arise when the technology is being used as intended but gives incorrect results, and harms following from (intentional or unintentional) misuse of the technology.
- If there are negative societal impacts, the authors could also discuss possible mitigation strategies (e.g., gated release of models, providing defenses in addition to attacks, mechanisms for monitoring misuse, mechanisms to monitor how a system learns from feedback over time, improving the efficiency and accessibility of ML).

11. Safeguards

Question: Does the paper describe safeguards that have been put in place for responsible release of data or models that have a high risk for misuse (e.g., pretrained language models, image generators, or scraped datasets)?

Answer: [NA]

Justification: The paper poses no such risks.

Guidelines:

- The answer NA means that the paper poses no such risks.
- Released models that have a high risk for misuse or dual-use should be released with necessary safeguards to allow for controlled use of the model, for example by requiring that users adhere to usage guidelines or restrictions to access the model or implementing safety filters.
- Datasets that have been scraped from the Internet could pose safety risks. The authors should describe how they avoided releasing unsafe images.
- We recognize that providing effective safeguards is challenging, and many papers do not require this, but we encourage authors to take this into account and make a best faith effort.

12. Licenses for existing assets

Question: Are the creators or original owners of assets (e.g., code, data, models), used in the paper, properly credited and are the license and terms of use explicitly mentioned and properly respected?

Answer: [Yes]

Justification: They are properly credited and respected in this paper.

Guidelines:

- The answer NA means that the paper does not use existing assets.
- The authors should cite the original paper that produced the code package or dataset.

- The authors should state which version of the asset is used and, if possible, include a URL.
- The name of the license (e.g., CC-BY 4.0) should be included for each asset.
- For scraped data from a particular source (e.g., website), the copyright and terms of service of that source should be provided.
- If assets are released, the license, copyright information, and terms of use in the package should be provided. For popular datasets, paperswithcode.com/datasets has curated licenses for some datasets. Their licensing guide can help determine the license of a dataset.
- For existing datasets that are re-packaged, both the original license and the license of the derived asset (if it has changed) should be provided.
- If this information is not available online, the authors are encouraged to reach out to the asset's creators.

13. New Assets

Question: Are new assets introduced in the paper well documented and is the documentation provided alongside the assets?

Answer: [NA]

Justification: The paper does not release new assets.

Guidelines:

- The answer NA means that the paper does not release new assets.
- Researchers should communicate the details of the dataset/code/model as part of their submissions via structured templates. This includes details about training, license, limitations, etc.
- The paper should discuss whether and how consent was obtained from people whose asset is used.
- At submission time, remember to anonymize your assets (if applicable). You can either create an anonymized URL or include an anonymized zip file.

14. Crowdsourcing and Research with Human Subjects

Question: For crowdsourcing experiments and research with human subjects, does the paper include the full text of instructions given to participants and screenshots, if applicable, as well as details about compensation (if any)?

Answer: [NA]

Justification: The paper does not involve crowdsourcing nor research with human subjects

Guidelines:

- The answer NA means that the paper does not involve crowdsourcing nor research with human subjects.
- Including this information in the supplemental material is fine, but if the main contribution of the paper involves human subjects, then as much detail as possible should be included in the main paper.
- According to the NeurIPS Code of Ethics, workers involved in data collection, curation, or other labor should be paid at least the minimum wage in the country of the data collector.

15. Institutional Review Board (IRB) Approvals or Equivalent for Research with Human Subjects

Question: Does the paper describe potential risks incurred by study participants, whether such risks were disclosed to the subjects, and whether Institutional Review Board (IRB) approvals (or an equivalent approval/review based on the requirements of your country or institution) were obtained?

Answer: [NA]

Justification: The paper does not involve crowdsourcing nor research with human subjects

Guidelines:

- The answer NA means that the paper does not involve crowdsourcing nor research with human subjects.
- Depending on the country in which research is conducted, IRB approval (or equivalent) may be required for any human subjects research. If you obtained IRB approval, you should clearly state this in the paper.
- We recognize that the procedures for this may vary significantly between institutions and locations, and we expect authors to adhere to the NeurIPS Code of Ethics and the guidelines for their institution.
- For initial submissions, do not include any information that would break anonymity (if applicable), such as the institution conducting the review.